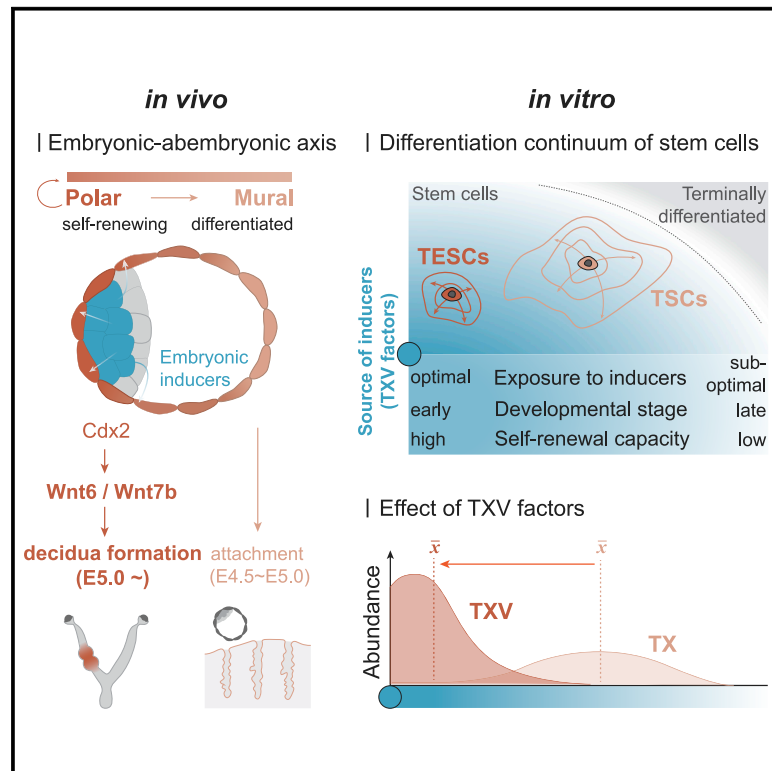# Epiblast inducers capture mouse trophectoderm stem cells *in vitro* and pattern blastoids for implantation *in utero*

Graphical abstract

Authors

Jinwoo Seong, Javier Frias-Aldeguer, Viktoria Holzmann, ..., Derk ten Berge, Niels Geijsen, Nicolas C. Rivron

Correspondence

nicolas.rivron@imba.oeaw.ac.at

In brief

Here, Seong et al. identify an optimal set of epiblast inducers that captures mouse trophectoderm stem cells (TESCs) as a stable and highly self-renewing state reflecting the blastocyst stage. TESCs have enhanced capacity to form blastoids that induce deciduae formation more efficiently *in utero* due to WNT6/7B secretion.

Highlights

- TSCs' heterogeneity reflects plastic transitions occurring during implantation

- Suboptimal inductions favor TSCs' heterogeneity and escape from self-renewal

- Optimal inducers capture TESCs reflecting blastocyst stage

- TESCs form more blastoids that better decidualize the uterus due to WNT6/7B secretion

CellPress

Article

Epiblast inducers capture mouse trophectoderm stem cells *in vitro* and pattern blastoids for implantation *in utero*

Jinwoo Seong,[1,7] Javier Frias-Aldeguer,[2,3,7] Viktoria Holzmann,[1,7] Harunobu Kagawa,[1] Giovanni Sestini,[1] Heidar Heidari Khoei,[1,4] Yvonne Scholte Op Reimer,[1] Maarten Kip,[2] Saurabh J. Pradhan,[1] Lucas Verwegen,[5] Judith Vivié,[2] Linfeng Li,[3] Anna Alemany,[2] Jeroen Korving,[2] Frank Darmis,[2] Alexander van Oudenaarden,[2] Derk ten Berge,[5] Niels Geijsen,[2,6] and Nicolas C. Rivron[1,2,3,8,*]

[1]Institute of Molecular Biotechnology of the Austrian Academy of Sciences, Vienna Biocenter, Vienna, Austria
[2]Hubrecht Institute for Developmental Biology and Stem Cell Research, Utrecht, the Netherlands
[3]Maastricht University, Maastricht, the Netherlands
[4]Department of Stem Cells and Developmental Biology, Cell Science Research Center, Royan Institute for Stem Cell Biology and Technology, ACECR, Tehran, Iran
[5]Department of Cell Biology, Erasmus MC, University Medical Center Rotterdam, Rotterdam, the Netherlands
[6]Department of Anatomy and Embryology, LUMC, Leiden University, Leiden, the Netherlands
[7]These authors contributed equally
[8]Lead contact
*Correspondence: nicolas.rivron@imba.oeaw.ac.at
https://doi.org/10.1016/j.stem.2022.06.002

SUMMARY

The embryo instructs the allocation of cell states to spatially regulate functions. In the blastocyst, patterning of trophoblast (TR) cells ensures successful implantation and placental development. Here, we defined an optimal set of molecules secreted by the epiblast (inducers) that captures *in vitro* stable, highly self-renewing mouse trophectoderm stem cells (TESCs) resembling the blastocyst stage. When exposed to suboptimal inducers, these stem cells fluctuate to form interconvertible subpopulations with reduced self-renewal and facilitated differentiation, resembling peri-implantation cells, known as TR stem cells (TSCs). TESCs have enhanced capacity to form blastoids that implant more efficiently *in utero* due to inducers maintaining not only local TR proliferation and self-renewal, but also WNT6/7B secretion that stimulates uterine decidualization. Overall, the epiblast maintains sustained growth and decidualization potential of abutting TR cells, while, as known, distancing imposed by the blastocyst cavity differentiates TR cells for uterus adhesion, thus patterning the essential functions of implantation.

INTRODUCTION

To implant into the uterus, mammals form a blastocyst comprising an inner epiblast (EPI) that later forms the body, surrounded by a fluid-filled, epithelial cyst called trophectoderm (TE) composed of trophoblasts (TRs) that will form the placenta. The EPI is placed asymmetrically in the TE cyst, a positioning that defines the first developmental axis (polar-mural, a.k.a. embryonic-abembryonic). Along this axis, the TE abutting the EPI (polar TE) proliferates and self-renews to progressively build the placenta into a composite organ that fulfills crucial functions (e.g., gas exchange, excretion of waste products, and functions that are immunological). The separation from the EPI, on the other hand, is associated with TE differentiation, decreased proliferation, and the capacity to attach to the uterus (Copp, 1978; Das et al., 1994; Gardner, 2000; Klaffky et al., 2001). Thus, one function of the blastocyst cavity is to separate the pools of TRs that will form the placenta or mediate the initial uterus attachment. In response to blastocyst implantation, uterine cells proliferate and undergo functional changes to create the decidua, a cocoon required for a successful

pregnancy. Faulty decidualization is associated with infertility and miscarriages (Cha et al., 2012).

The TR lineage develops in a different way as compared to the EPI lineage: while the EPI lineage progress through pluripotency via a sequence of irreversible and epigenetically engraved lock steps with different signaling requirements (Nichols and Smith, 2012), TR progenitors self-renew *in vivo* thanks to a niche environment generated at the EPI/TR interface. This environment is currently defined by a number of soluble (Guzman-Ayala et al., 2004) and extracellular matrix (Kiyozumi et al., 2020) molecules that promote proliferation while inhibiting precocious differentiation, thus maintaining self-renewal. FGF4 is a niche factor produced by the EPI starting in mid-stage blastocysts (E3.25; Guo et al., 2010; Ohnishi et al., 2014) whose importance is evidenced by $Oct4^{-/-}$ mutant blastocysts that fail to express FGF4 but respond to exogenous FGF4 by increasing TR proliferation (Nichols et al., 1998). FGF4 induces the phosphorylation of ERK in some of the polar TE cells (E3.25–4.5) (Azami et al., 2019), which promotes proliferation and prevents differentiation and apoptosis (E4.5–5.0) through FGF receptors (Chai et al., 1998), FRS2 (Gotoh

et al., 2005), SHP2 (Yang et al., 2006), and the signaling effector kinase ERK2 (Hatano et al., 2003; Saba-El-Leil et al., 2003). During implantation, a tissue descending from the polar TE, the extraembryonic ectoderm (ExE), maintains the TR progenitors and has a continuous requirement for ERK signals between at least E4 and E8 (Corson et al., 2003; Azami et al., 2019). TGFβ superfamily members also contribute to the post-implantation maintenance of TR progenitors through activity of the Nodal receptor ACVR1B (Gu et al., 1998), the Nodal pro-protein convertases PCSK6 (PACE4) (Constam and Robertson, 2000) and Furin (Roebroek et al., 1998), and the effectors SMAD1 (Aubin et al., 2004) and SMAD2 (Weinstein et al., 1998). Finally, the Hippo and Notch pathways are important regulators of the initial TE specification (Nishioka et al., 2009; Rayon et al., 2014), and IGF2 is expressed at high levels in the polar TE (Nakamura et al., 2015), ExE, ectoplacental cone (EPC), allantois, and chorion (Lee et al., 1990) and contributes to TR proliferation (Gardner et al., 1999; Constância et al., 2002; Zechner et al., 2002).

The EPI/TR interface is a dynamic and regulative environment: the EPI sustains FGF4 production that stimulates BMP4 secretion from the ExE (Lawson et al., 1999; Murohashi et al., 2010) that might act as a direct niche factor (; Graham et al., 2014; Rivron et al., 2018) but also indirectly induces the EPI to express Nodal and Wnts (E6) (Ben-Haim et al., 2006; Miura et al., 2010). Nodal and Wnt ligands act in autocrine ways on the EPI but also feed back onto the TR progenitors to maintain self-renewal in part by regulating FGF4 expression (Guzman-Ayala et al., 2004; Ben-Haim et al., 2006). Altogether, this interface is a hotspot of regulative interactions maintaining the TR progenitors that are thought to persist until the mid-gestation placenta (Guzman-Ayala et al., 2004; Ueno et al., 2013; Natale et al., 2017).

In the presence of FGF4, TR progenitors isolated either from the blastocyst (E4.5) or ExE (E6.5) can proliferate and self-renew *in vitro* as TR stem cells (TSCs) (Tanaka et al., 1998). This shows that these progenitors possess an intrinsic, long-term self-renewal potential maintained by an EPI inducer. Here, we show that TSCs, which are notoriously heterogeneous (Sebastiano et al., 2010; Wu et al., 2011; Ohinata and Tsukiyama, 2014; Kuales et al., 2015; Motomura et al., 2016; Perez-Garcia et al., 2021), comprise fluctuating, interconvertible subpopulations resembling peri-implantation TRs. However, an optimal set of EPI inducers captures stable, highly self-renewing TRs resembling the blastocyst TE. We term these lines trophectoderm stem cells (TESCs). We show that TESCs not only maintain a high self-renewing capacity while inhibiting precocious differentiation but also secrete Wnt ligands that contribute to the decidual reaction *in utero*. Observing the behavior of TESCs and TSCs, we argue that optimal exposure to inducers sustains high self-renewal after implantation, while suboptimal exposure enables the concomitance of interconvertible subpopulations facilitating the exit from self-renewal and differentiation.

RESULTS

The transcriptome of pre- and post-implantation trophoblast cell types

In late mouse blastocysts, the transcription factor (TF) Caudal Type Homeobox 2 (CDX2) (Donnison et al., 2005; Strumpf et al., 2005) marks the polar TE. We confirmed that CDX2 expression decreases in the mural TE of E4.5 blastocysts, while KRT18 increases (mRNA and protein levels, Figures 1A and S1A). We first analyzed the transcriptomes of peri-implantation TRs to identify hallmarks for these states and candidate signaling pathways regulating them. Unsupervised clustering of E4.5 TE cells (late blastocyst stage) using an existing single-cell mRNA sequencing (scRNA-seq) dataset (Nakamura et al., 2015) confirmed a transcriptomic distinction between polar and mural TE (Figure 1B). We identified 2,107 differentially expressed genes (DE-Gs) (average LogFC ±0.25, p < 0.05, Figure S1B and Table S1A). Polar TE had increased expression of TFs regulating TR self-renewal (Cdx2, Esrrb, and Elf5) (Donnison et al., 2005; Strumpf et al., 2005; Gao et al., 2018), Wnt ligands Wnt7b and BMP1/4/8b, and the receptor Il6st (Figure 1D). Consistent with the established role of the MAPK pathway in regulating TR proliferation (Nichols et al., 1998; Tanaka et al., 1998), we found a pathway enrichment (Fgfr1, Mapk1, Map2k1, Grb2, and Spry2) and an upregulation of the proliferation machinery (Cdk1, Ccnb1-2, Ccnd1, Mki67, and Pcna) (Figures 1C and 1D). Polar cells also more abundantly expressed effectors of the SMAD signaling pathway (E2f4, Smad3, Smad4, and Smad7) (Nakao et al., 1997; Ishisaki et al., 1999) and Pcsk6, a secreted pro-convertase that cleaves the TGFβ family member pre-Nodal to locally enhance its potency. This supports an earlier role for SMAD signaling than previously reported (Tsuji et al., 2003; Guzman-Ayala et al., 2004; Mesnard et al., 2011). Similarly, Hippo pathway members (Amot, Lats2, Ywhab, and Wwc1) and targets (Max, Myc, and Ccnd1) that regulate Cdx2 were also more abundant in the polar TE (Figures 1C, 1D, and S1C). We confirmed the presence of FGF4, BMP4, Nodal, and IL11 transcripts in the blastocyst EPI by single-molecule FISH (smFISH) (IL11 is also detected in the TE, Figure S1D). Finally, ERK, SMAD1/5/8, and STAT are phosphorylated in the TE, although ERK is restricted to few TRs (Figure S1D). We concluded that, beyond FGF signaling, the STAT, SMAD, and Hippo pathways are enhanced in the polar TE. We also extracted markers of the polar region (Ly6a, Gsto1, and Ddah1, Figure 1D and Table S1A) for their high expression. Mural TE had increased expression of integrins (Itga5/6/7/v), laminins (Lama1/b1/b2), galectins (Lgals1 and Lgalsl), Hb-egf, and ephrins (Efna1/b1/b2), consistent with an adhesive and repulsive/invading phenotype initiating implantation (Klaffky et al., 2001; Sutherland, 2003; Barrientos et al., 2014) (Figure S1C). The mural TE was additionally characterized by molecules associated with the formation of intermediate filaments (Krt8/18) and tight junctions (Ocln, Pard3, and Pard6b/g) and by TFs Gata2, Klf4/5/9, Tfap2a, and Tcf7l2 (Figure 1D).

High CDX2 expression also marks the post-implantation ExE (E6.5), while KRT18 is strongly expressed in surrounding cells (Figure 1E). When we compared the transcriptome of TE and ExE TRs using another published metadata set (Posfai et al., 2021) (Figures 1F and S1E–S1H), we identified 2,971 DE-Gs (average LogFC ±0.25, p < 0.05, Figure S1E and Table S1B), inferring differences in cell-cycle regulation and cell-cell adhesion (Figure S1I). Developmental progression was reflected by increased expression of Elf5, Tead2, Id1, Cited2, Ascl2, Eomesodermin (Eomes), Hand1, and Sox2 and decreased expression of Cdx2, Klf5, Tead4, Gata2/3, Ly6a, and Spry2 TFs (Figure S1J). Expression of the secreted ligands Bmp4 and Igf2 increased, whereas genes associated with insulin signaling decreased.
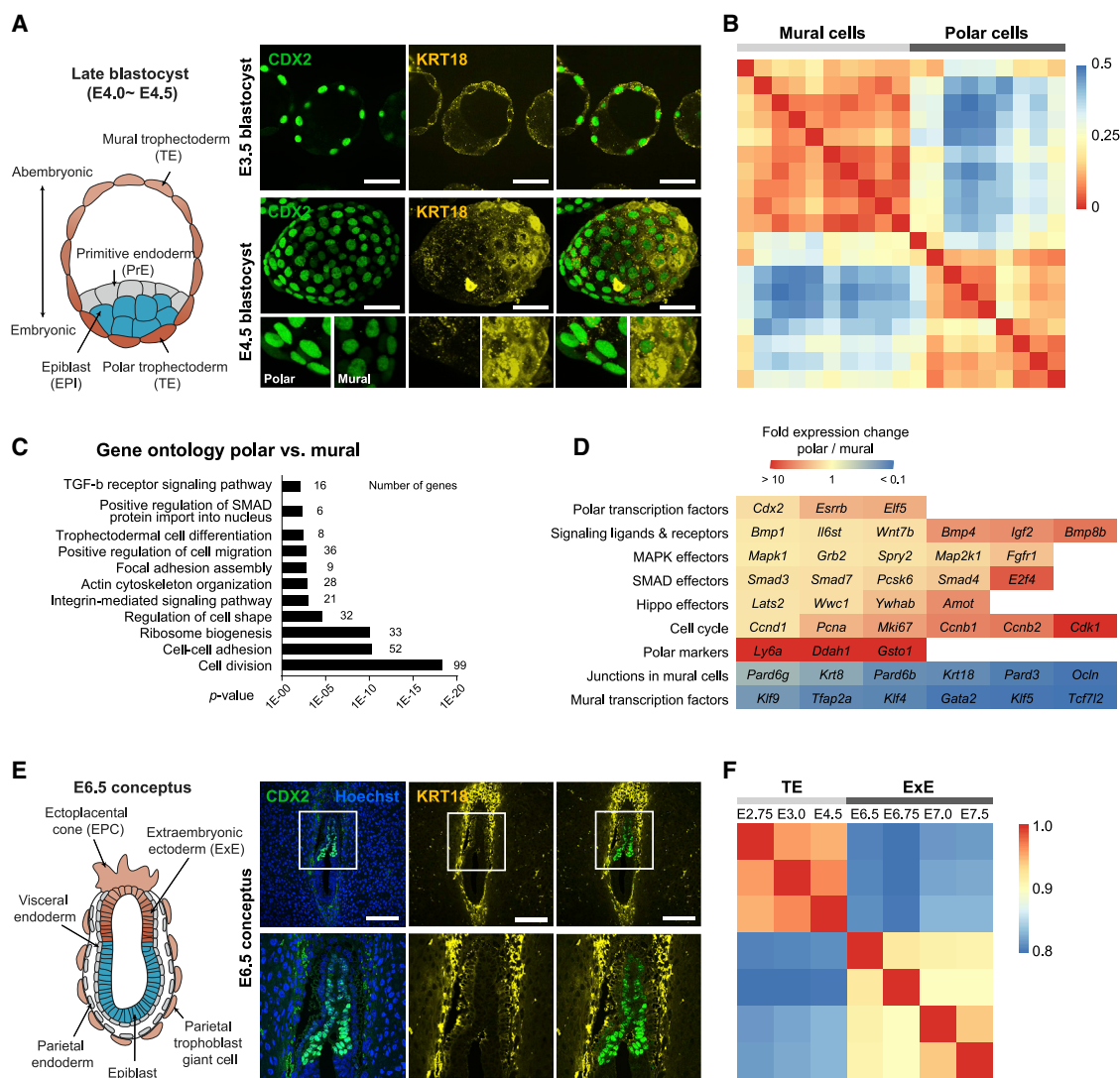
Figure 1. The transcriptomic transitions of pre- and post-implantation TRs

(A) Immunostaining for CDX2 and KRT18 showing uniform protein distribution at E3.5 but polar or mural bias in E4.5 blastocysts. Higher CDX2 expression in the polar region was detected in 65% of late blastocysts (11/17). Scale bar, 40 μm.

(B) Unsupervised clustering analysis (distance map from RaceID pipelines) of E4.5 TE single cells confirms the presence of two subpopulations: polar and mural. Each column and row represent a single cell from each group.

(C) Gene ontology analysis based on differentially expressed genes between polar and mural TE.

(D) Heatmap showing fold expression changes of indicated genes in the polar TE compared to the mural TE (see also Table S1).

(E) In an E6.5 (post-implantation) conceptus, CDX2 expression is restricted to the ExE and does not correlate with KRT18 localization. Scale bar, 150 μm.

(F) Spearman correlation analysis of TE and ExE at various developmental stages shows transcriptomic differences between TE and ExE.

See also Figure S1.

Altogether, this analysis highlights specific EPI inducers, TRs signaling pathway activities, and markers that define TR progression around implantation time.

Trophoblast stem cells encompass multiple subpopulations reflecting the trophectoderm, extraembryonic ectoderm, and differentiated trophoblasts

TSCs' intercellular heterogeneity has been visualized by CDX2 and EOMES immunofluorescence (Figure 2A) (Kuales et al.,

2015; Motomura et al., 2016). To resolve transcriptional profiles of subpopulations, we performed bulk RNA-seq of 1,000 CDX2^{high} and CDX2^{low} TSCs derived from a CDX2-eGFP reporter mouse line (McDole and Zheng, 2012) (Figure 2B) and cultured in chemically defined medium complemented with FGF4/TGFβ1 (TX medium; Kubaczka et al., 2014), which are the minimal molecules necessary for maintaining *in vitro* TR proliferation and self-renewal. We identified 1,941 DE-Gs (FC > 1.5, p < 0.01, Table S2). CDX2^{high} TSCs were enriched for TFs regulating self-renewal (*Esrrb*, *Eomes*, and *Elf5*),
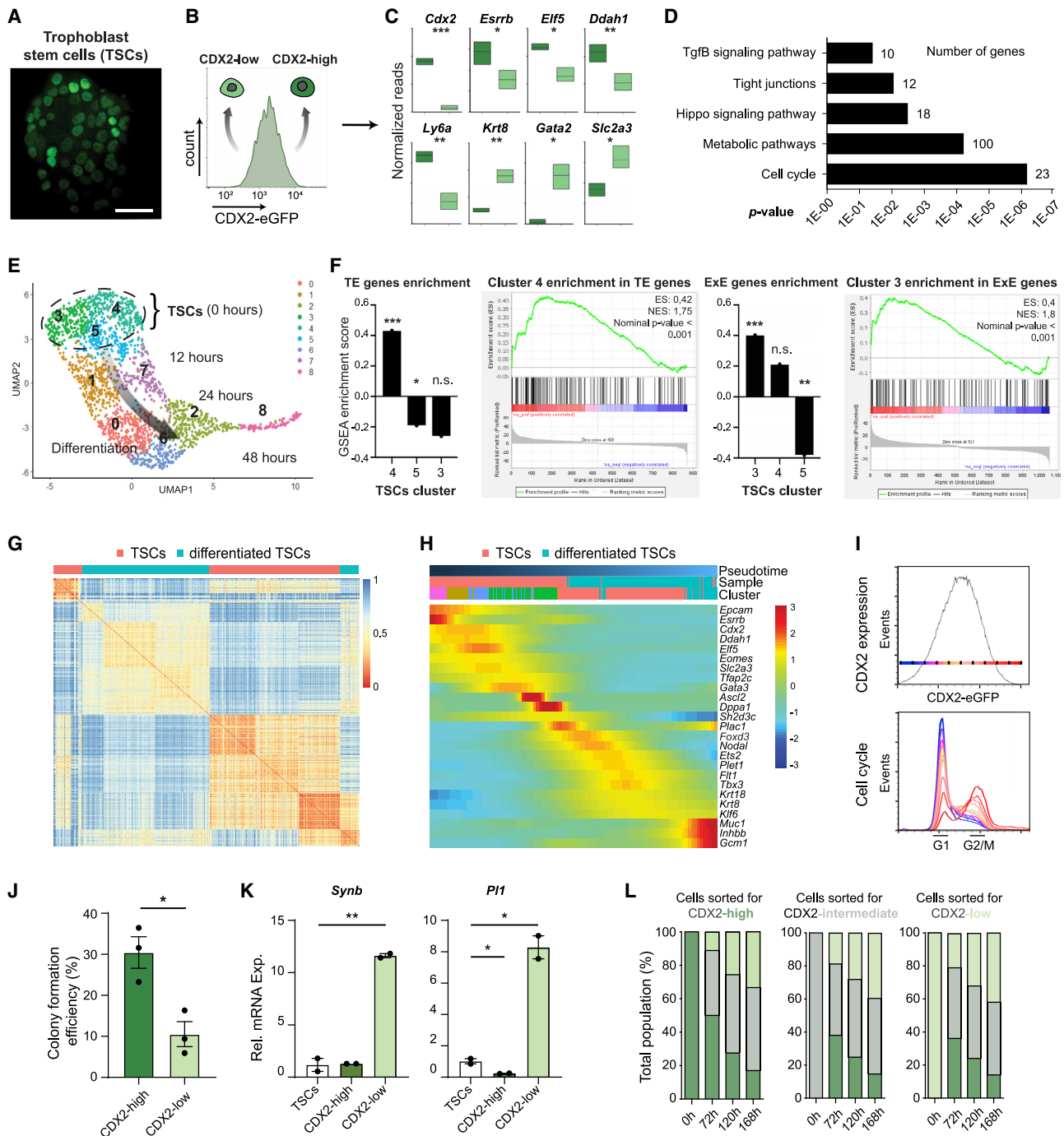
Figure 2. TSCs comprise heterogeneous and interconvertible states reflecting peri-implantation stages

(A) Naive GFP signal of CDX2-eGFP TSCs. Scale bar, 40 μm.

(B) CDX2^{high} and CDX2^{low} TSCs were sorted out with flow cytometry for RNA-seq.

(C) mRNA expression of self-renewal, polar, and differentiated marker genes in CDX2^{high} and CDX2^{low} TSCs (based on three independent bulk RNA-seq results). Dark and light green represent CDX2^{high} and CDX2^{low} TSCs, respectively.

(D) Gene ontology analysis based on differentially expressed genes enriched in CDX2^{high} compared to CDX2^{low} TSCs.

(E) Single-cell transcriptome analysis upon removal of minimal inducers.

(F) Gene set enrichment analysis (GSEA) for TE and ExE genes. Clusters 3, 4, and 5 are considered to be TSCs and show different gene enrichment, indicating heterogeneity of TSCs. Data were analyzed by Wilcox likelihood-ratio test.

(G) Unsupervised cell clustering analysis (distance map) of TSCs and 6-day-differentiated TSCs.

(legend continued on next page)

cell-cycle components, the Hippo pathway, and some polar markers (*Ly6a* and *Ddah1*). In contrast, the CDX2^{low} TSCs showed higher expression of differentiation markers *Krt8* and *Gata2* (Figures 2C and 2D).

Next, we delineated TSCs' heterogeneity through scRNA-seq analysis (Figures 2E and S2A). Three subpopulations (cluster 3, 4, and 5) were present (Figure 2E). One of these clusters (cluster 4) was enriched for TE-associated genes (GSEA, Normalized Enrichment Score [NES]: 1.75; e.g., *Gata3* and *Ly6a*), including genes associated with epithelia (*Cldn4/6*, *Krt18*, *Epcam*, *Ctnna1*, *Lgals9, Krt8/18*, and *Itga6*) (Table S3A). Another cluster (cluster 3) was enriched for ExE genes (GSEA, NES: 1.8; e.g., *Eomes*, *Elf5*, *Hand1*, *Tead2*, *Id1*, *Cited2*, and *Bmp4*) (Figures 2F and S2B and Table S3B). The third one (cluster 5) was significantly depleted in both TE and ExE genes (Figure S2C) and reflected more differentiated TRs. Upon removal of FGF4/TGFβ1, cells differentiated as indicated with a decrease in self-renewal and TE-related transcripts and an increase in differentiation-associated transcripts (Figure S2D).

By analyzing single TSCs and 6-day-differentiated TSCs, we obtained a different resolution of the heterogeneity profile. Unsupervised clustering analysis separated TSCs into four subpopulations and 6-day-differentiated TSCs into two subpopulations (Figure 2G). Cells aligned along a Monocle-predicted pseudotime trajectory (Figures 2H and S2E) (Trapnell et al., 2014) in which low pseudotime values corresponded to a TSC subpopulation with higher *Cdx2* and *Esrrb* expression levels, while the next cells along pseudotime values showed higher expression of *Elf5*, consistent with ExE identity (Figure 2H). Following in the trajectory were cells abundant for *Tfap2c* and *Ascl2* expression and TFs marking the ExE/EPC (Guillemot et al., 1994; Auman et al., 2002; Werling and Schorle, 2002; Latos et al., 2015), while the highest pseudotime values marked cells expressing the TR differentiation markers *Flt1* or *Gcm1*. Importantly, we identified differentiated TRs within TSCs (9%, Figure S2E), showing that FGF4/TGFβ1 consent to spontaneous differentiation. We confirmed the presence of subpopulations using smFISH with cells rich in either *Cdx2*, *Gsto1*, and *Esrrb* or *Ascl2*, *Gcm1*, and *Krt18* transcripts (Figure S2F). This was further confirmed at the protein level (CDX2/KRT18, Figure S2G). Taken together, these analyses show that FGF4/TGFβ1 consent to the maintenance of concomitant subpopulations reflecting the blastocyst TE, post-implantation ExE, and more differentiated TRs.

Trophoblast stem cells' subpopulations reflect functionally different and interconvertible stem cell states

Next, we examined whether CDX2^{high} and CDX2^{low} TSCs represent functionally different states. Using flow cytometry analysis, we observed that CDX2^{high} cells were present in all cell-cycle phases, while CDX2^{low} cells were predominantly in the G0/G1 phases (Figure 2I). Consistently, CDX2^{high} cells had a 30% clonogenicity rate, three times higher than that of CDX2^{low} cells (Figure 2J), which were more prone to differentiate upon removal of FGF4/TGFβ1 (*Pl1* and *Synb* mark TR giant cells and syncytiotrophoblasts, respectively; Figure 2K).

Protein fluctuation can occur stochastically but synchronously for members of the same biological pathway, which generates heterogeneity (Sigal et al., 2006). When we conducted live imaging of CDX2-eGFP TSCs, we observed transitions between the CDX2^{high} and CDX2^{low} states (Figure S2I and Video S1) reminiscent of fluctuations in ESCs (Chambers et al., 2007; Hayashi et al., 2008; Hastreiter et al., 2018). Thus, we investigated whether subpopulations were capable of interconversion. Within 5 days after sorting of CDX2^{high} or CDX2^{low} cells, these subpopulations reestablished the initial heterogeneity (Figure 2L), and analysis of multiple sortings over 50 days showed that the initial transcriptome was restored (Figures S2I and S2J). We concluded that these states are reversible and that heterogeneity is an intrinsic, possibly regulated property of TSCs under minimal conditions. However, the CDX2^{low} cells proliferated more slowly than the CDX2^{high} cells (Figure S2K), suggesting a priming mechanism.

In ExE and TSCs, the *Cdx2* locus is marked with high levels of the activating H3K4me3 mark, while these levels decrease upon differentiation (Rugg-Gunn et al., 2010). Accordingly, H3K4me3 levels at the *Cdx2* promoter were 50% lower in CDX2^{low} TSCs, suggesting either reduced promoter activity or fewer active promoters (Figure S2L). In contrast, levels of the active transcription marker H3K9Ac were comparable between populations. We concluded that the *Cdx2* locus remains accessible and can be reactivated, for example in response to an environmental factor such as a growth factor, but is subjected to reversible epigenetic regulations that prime CDX2^{low} TRs for differentiation. This transcriptomic and epigenetic reversibility is consistent with the reversibility of the mural TE, as shown by blastocyst microdissection/recombination (Gardner et al., 1973; Gardner, 1983). Overall, we concluded that FGF4/TGFβ1 allow fluctuating, interconvertible, peri-implantation-like TR states with different proliferation and self-renewing potentials, a phenomenon that facilitates differentiation.

Exposure to optimal embryonic inducers generates stable CDX2^{high} trophoblast stem cells

Next, we investigated the impact of combined EPI inducers. We tested individual molecules acting on pathways found active in the TE (Figure S1D) for their capacity to induce CDX2 in TSCs (Figures 3A and S3A and Table S4). Nine molecules acted in a dose-dependent manner including IL11, Activin, BMP4/7, 1-Oleoyl Lysophosphatidic Acid (LPA) (Yu et al., 2012, 2021; Goto et al., 2015), 8-Br cAMP, XAV939, and the PPAR

(H) Pseudotime heatmap for visualization of expression patterns along with marker genes for various differentiation states. For clusters, see also Figure S2E.
(I) Cell-cycle analysis of TSCs shows a correlation between CDX2 expression (higher CDX2 content in red, lower in blue) and the cell-cycle state.
(J) Colony formation potential of single CDX2^{high} and CDX2^{low} cells based on three independent experiments. Data are means ± SEM, analyzed by Student's t test.
(K) mRNA expression of differentiated marker genes in CDX2^{high} andCDX2^{low} TSCs.
(L) Percentage of the different subpopulations upon pure subpopulation sorting and further independent culture, based on three independent experiments and a total of 96 wells of cells for each condition. Dark green for CDX2^{high}, gray for CDX2^{intermediate}, light green for CDX2^{low}.
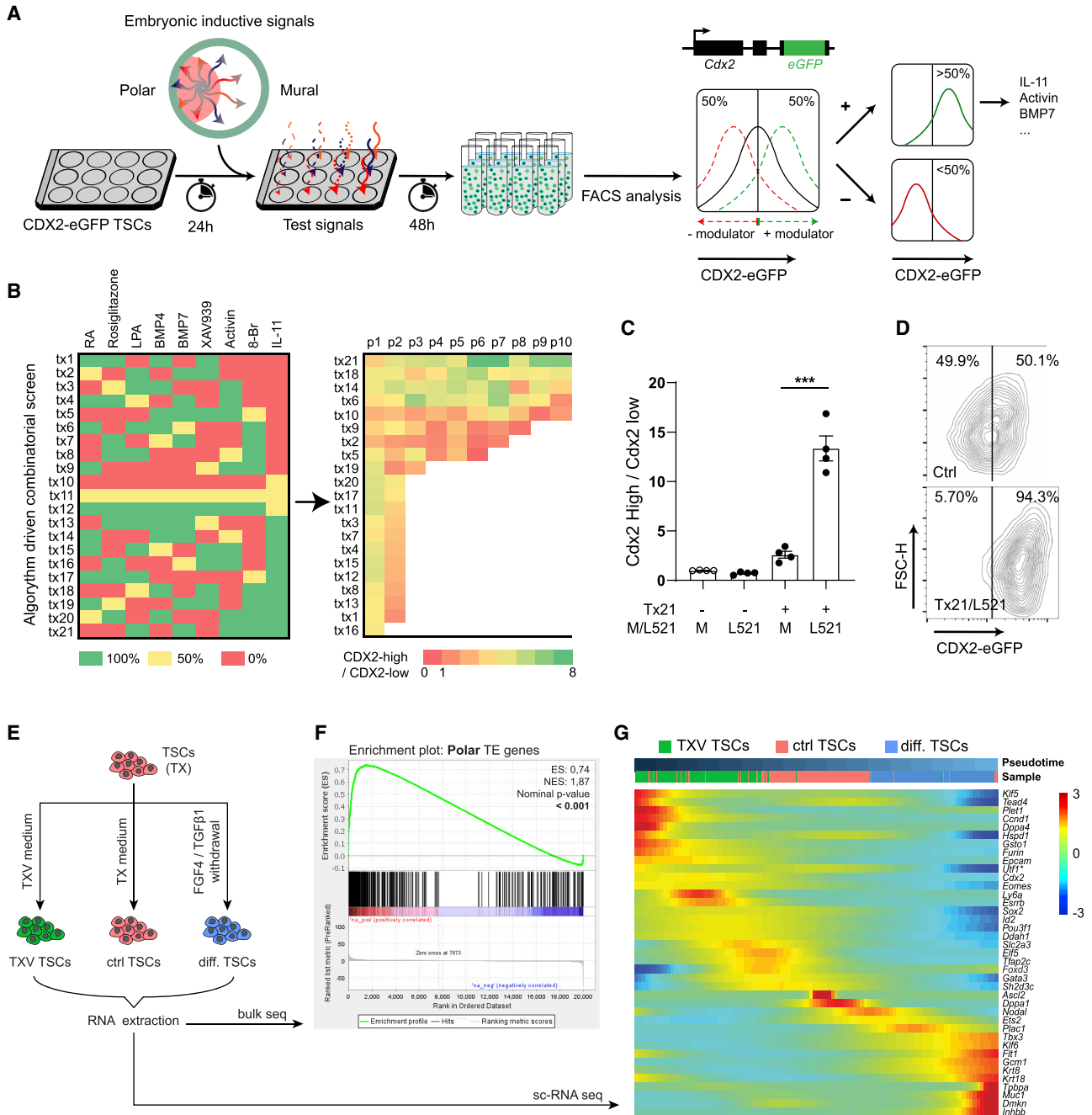For each panel, *p < 0.05, **p < 0.01, ***p < 0.001. See also Figure S2.

Figure 3. Optimal embryonic inducers capture TR stem cells with a transcriptome more akin to the TE

(A) Strategy to identify CDX2 expression regulators with CDX2-eGFP TSCs. Chemicals with a CDX2^{high}/CDX2^{low} ratio bigger than 1.25 were considered positive modulators.

(B) List of 21 different cocktails using a combination of nine different CDX2 regulators (left). Green, yellow, and red color with percentage indicate the relative concentration of each modulator. Actual modulator concentrations are indicated in Figure S3A. The 21 cocktails were ranked based on the average CDX2^{high}/CDX2^{low} ratio after 10 passages (right). Colors from 0 to eight indicate CDX2^{high}/CDX2^{low} ratio based on flow cytometry.

(C) CDX2^{high}/CDX2^{low} ratios of TSCs upon combination of the top cocktail (Tx21) with either Matrigel or Laminin 521 (L521) coated plates. Data are means ± SEM, analyzed by one-way ANOVA. ***$p < 0.001$.

(D) Flow cytometry showing that Tx21 compounds combined with L521 dramatically increase the percentage of CDX2^{high} cells.

(E) Schematic view of each group preparation.

(F) GSEA for polar TE genes with TSCs exposed to optimal inducers for 15 days.

(G) Pseudotime heatmap for visualization of expression patterns along with self-renewal, polar, differentiated, and classical TSCs marker genes. Most self-renewal and polar genes are enriched in TXV TSCs compared to TX or differentiated TSCs.

See also Figure S3.

receptor agonist Rosiglitazone) (CDX2^high/CDX2^low ratio >1.25, Table S4). We excluded the autocrine factor IGF2, previously proposed to guide TR differentiation (Lee et al., 2019) (Figure S3B). Because secreted molecules act synergistically during development, we explored combinations using factorial design (Hutchens et al., 2007) by culturing TSCs for 10 passages while monitoring CDX2 expression (Figure 3B). Although all combinations initially induced CDX2, most cultures (17/21) collapsed after two passages due to a lack of proliferation or attachment. The remaining four conditions supported a sustainable, long-term increase in CDX2 expression without apparent cell death. Through principal component analysis, we identified IL11, BMP7, LPA, Activin, and 8-Br cAMP (Tx21 medium) as most beneficial, evidenced by higher expression of self-renewal TFs (*Cdx2*, *Eomes*, *Esrrb*, and *Elf5*) and lack of upregulation of differentiation markers (e.g., ExE/EPC marker *Ascl2*) (Figures S3C–S3E). We then tested eight different laminin proteins to replace Matrigel, and we selected laminin L521 based on its expression in the blastocyst, its support of TSC proliferation, and an increase of CDX2 expression (Figures 3C, 3D, and S3F–S3H). An optimal set of molecules includes FGF4 (25 ng/mL), TGFβ1 (2 ng/mL), Activin (50 ng/mL), IL11 (50 ng/mL), BMP7 (25 ng/mL), 8-Br cAMP (200 μM), LPA (5 nM), and L521 coating, hereafter referred to as TXV (for TX plus five compounds).

Trophoblast stem cells exposed to optimal epiblast inducers maintain a trophectoderm-like transcriptome

We next analyzed the transcriptome of TXV TSCs. In-bulk analyses showed that a transcriptome shift occurred within 48 h and was further enhanced after 15 days (1,360 and 3,473 DEG, respectively, p < 0.05) (Figure S3I and Tables S5AA, Tables S6AS6B, and S7). After 15 days, GSEA showed that polar TE genes were significantly enriched, including *Cdx2*, *Eomes*, and *Ly6a*, whereas mural and ExE genes were not (Figures 3E, 3F, and S3J). Notably, transcripts for molecules reported to mediate mural TE/endometrium interactions (*Lgals1*, *Hb-egf*, and *Efna1*) (Fujii et al., 2006; Lim and Dey, 2009; Barrientos et al., 2014; You et al., 2018) (Figure S3K) and transcripts for molecules that increase upon ExE progression (*Elf5*, *Tead2*, *Id1*, *Ascl2*, and *Hand1*) (Figure S1J) were decreased (Table S6A). Gene ontology analysis showed differences in transcription (448 genes, Benjamini = 1.4×10^{-12}), cell-cell adhesion (79 genes, Benjamini = 3.9×10^{-12}), and cell cycle (159 genes, Benjamini = 8.7×10^{-6}) (Tables S5A and S6A). A transcriptome shift was confirmed in three lines from different genetic backgrounds (Figure S3L).

Exposure to increased FGF4 concentrations or genetic induction of *Cdx2* (48 h, Figure S3J) led to different transcriptome shifts as compared to TXV (Tables S5B, S6B, S6C, and S7), which suggests that the set of inducers acts more broadly, possibly on CDX2 upstream regulators such as Notch signaling (*Notch4* and *Rbpj*) (Figure S3I and Tables S5B, S6B, S6C, and S7). scRNA-seq analysis (unsupervised clustering and monocle analysis) assigned the lowest pseudotime values to TXV TSCs and reflected a developmental trajectory with initially high expression of TE TFs (*Cdx2*, *Eomes*, and *Elf5*) and polar markers (*Ly6a*, *Ddah1*, *Hspd1*, *Gsto1*, and *Utf1*) (Figures 3G, S3M, and S3N). Cells with the lowest pseudotime values expressed high levels of *Klf5* and *Tead4*, two TFs essential for early TE specifica-
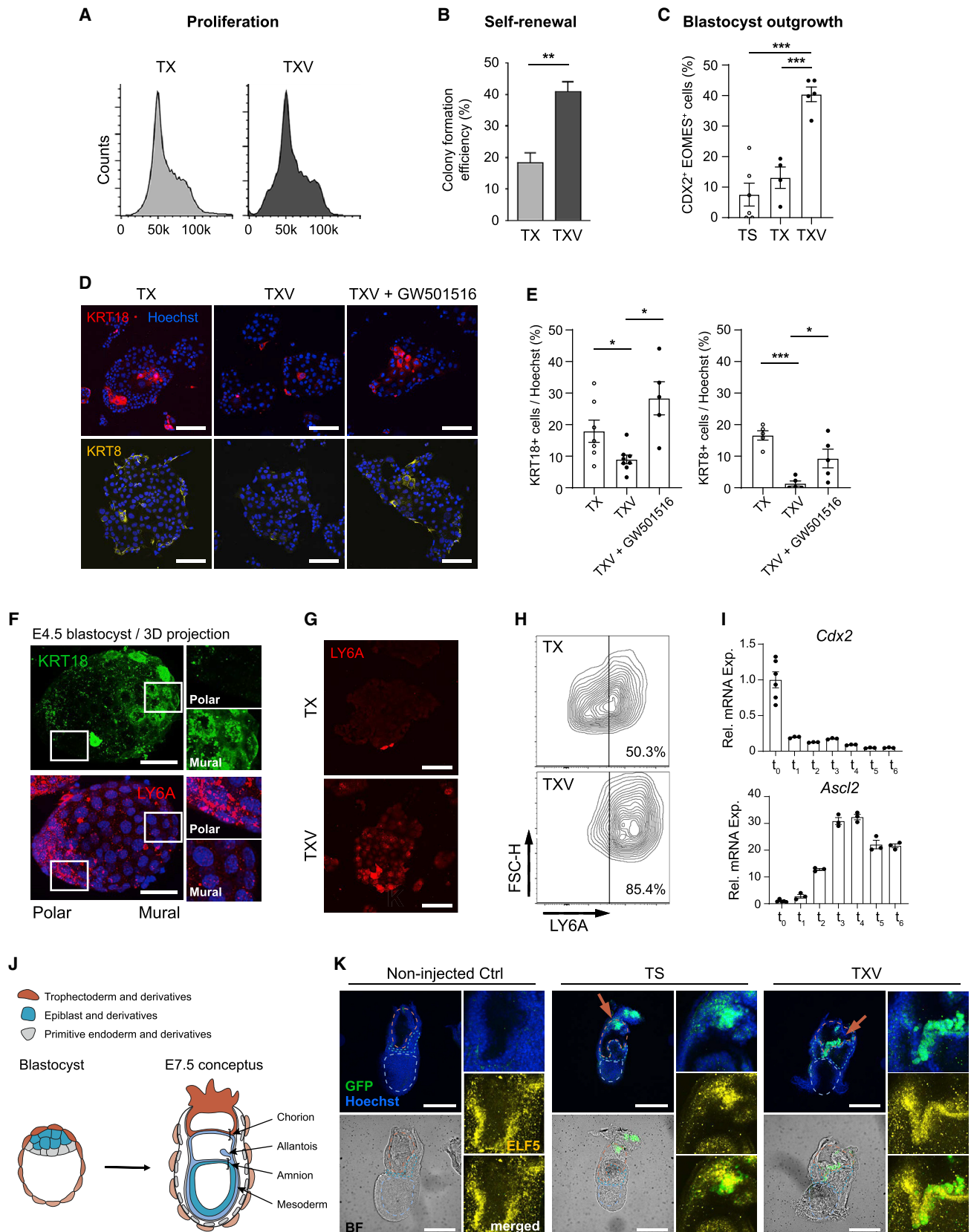
tion (Shindo et al., 2002; Yagi et al., 2007; Ema et al., 2008; Nishioka et al., 2008; Lin et al., 2010). These were followed by cells highly expressing the polar TE markers *Ly6a* and *Esrrb*, and *Duox2* and *Gsto1*, previously described as markers for *bona fide* TR progenitors (Kubaczka et al., 2014; Kuales et al., 2015) (Figure S3N). TE epithelia genes were also prominent at low pseudotime value (Figure S3O). Collectively, we concluded that an optimal set of EPI inducers (MAPK, Hippo, SMAD, and STAT; see Table S5A) maintain a state better reflecting the TE transcriptome and prevent the expression of blastocyst mural TE and post-implantation ExE genes.

Epiblast inducers enhance trophoblast stem cells' self-renewal, enhance derivation of lines, and repress differentiation

Culturing TSCs in TXV enhanced clonogenicity (40%, 2-fold, p < 0.0028; Figures 4A and 4B), mirroring levels of ground state ESCs (Ying et al., 2008). We also measured increased efficiency for TR progenitor derivation from blastocysts (percentage of CDX2^+/EOMES^+ cells, Figures 4C, S4A, and S4B) in the three different genetic backgrounds tested, including C57BL/6J mice (Ohinata and Tsukiyama, 2014). Cell line derivation was highly efficient from both E3.5 blastocysts and E6.5 isolated ExE (Figure S4C), showing the reversibility of ExE progenitors. In these lines, the number of differentiated KRT8/18^high cells reduced (2%–8%) and increased upon exposure to the PPARd receptor agonist GW501516 that confers TE implantation competency (Xie et al., 2008) (Figures 4D and 4E). The polar protein LY6A was also increased (Figures 4F–4H and S4E). Upon growth factor removal, TXV TSCs differentiated as evidenced by a decrease in *Cdx2* expression (day 1) and upregulation of the ExE/EPC marker *Ascl2* (day 2–3) (Figure 4I). Although TX TSCs required a transition to serum-containing medium to chimerize the placenta (Kubaczka et al., 2014), TXV TSCs contributed to the TE when injected into morula-stage embryos (Figure S4F) and chimerized the ELF5^+ ExE compartment (E7.5, Figures 4J, 4K, and S4G–S4I). We did not observe embryonic contribution.

Epiblast inducers enhance the epithelial phenotype and morphogenetic potential of trophoblast stem cells

The transcriptome of TXV TSCs was enriched in epithelia transcripts including those related to extracellular matrix organization, cell adhesion, pathways related to ECM-receptor interaction, focal adhesion, cytoskeleton, and tight junctions (e.g., *Cldn4*, *Cldn6*, *Tjp2*, and *Jam2*) that contribute to TE morphogenesis (Moriwak et al., 2007) (Figure S3O). By quantifying phenotypic changes of single-cell morphologies using E-CADHERIN/Hoechst-staining segmentation, we extracted 161 morphometric features from both TX TCSs (502 cells) and TXV TSCs (297 cells) (Figure S5A). After being ranked based on the p value scores (Mann-Whitney; Methods S1), the top 20% morphometric features separated the two populations (Figures S5B and S5C). TXV TSCs had significantly larger cell size and nuclei areas and were more circular and less lobulated (Figure S5D). Cells reflecting the TE should efficiently undergo epithelial morphogenesis. As compared to TX TSCs, TXV TSCs more efficiently formed blastoids that were larger and more circular (Figures 5A–5D and S5E). This was partly due to an enhanced autonomous potential measured by a higher capacity to

A Proliferation

B Self-renewal

C Blastocyst outgrowth

D

E

F E4.5 blastocyst / 3D projection

G

H

I

J

K Non-injected Ctrl · TS · TXV

form trophospheres (cavitation efficiency and circularity) (Figures S5F–S5H). This was also due to an enhanced response to ESCs as TXV TSCs formed blastoids that had a larger diameter, a feature that did not occur in trophospheres (Figures 5B and S5G). Because TX and TXV TSCs proliferate at similar rates in blastoids (Figure S5I), we concluded that the increased diameter was due to enhanced swelling in response to inducers. Blastoids correctly localized the basal adherens junctions (E-CADHERIN [E-CAD]) and apical cytoskeletal protein (KRT8/18) (Figure 5E). Taken together, these observations show that TXV TSCs have an enhanced epithelial phenotype and morphogenetic functions, consistent with the TE.

Cumulatively, we showed that TSCs cultured in TXV (1) enhance their transcriptomic similarity to the TE, (2) enhance their self-renewal, (3) repress gene expression associated with differentiation, (4) maintain their potential to rapidly differentiate and chimerize the ExE, and (5) have an enhanced potential to recapitulate features of TE epithelial morphogenesis. Therefore, we call these cells TESCs.

Epiblast inducers spatially pattern the polar-mural axis

Next, we asked whether inducers spatially pattern the polar- and mural-like states that confer specific functions during implantation. Single TRs isolated from blastoids formed a pseudotime trajectory (Figure S5J) that included three transitioning clusters (Figure S5K). Cells with low pseudotime values more abundantly expressed transcripts for *Esrrb*, *Cdx2*, and *Ly6a* (Figures 5F and 5G) and numerous polar genes (*Ly6a*, *Gsto1*, *Ddah1*, *Utf1*, and *Duox2*). In contrast, the cluster with the highest pseudotime value showed enhanced expression levels of mural markers (*Krt8/18*, *Ndrg1*, *Basp1*, *Ctsb*, *Flt1*, and *Slc5a5*) and of *Lgals1*, which mediates endometrial interaction (Sood et al., 2006; Shi et al., 2013; Barrientos et al., 2014) (Figure 5F). Using smFISH, we confirmed that the polar marker *Ly6a* was more prominently expressed in the blastoid polar cells (7/10) (Figures 5H and S5L). At the protein level, the axis defined by CDX2 and KRT8/18 formed at a low efficiency similar to that in previously reported blastoids formed either with ESCs (Rivron et al., 2018) or with EPSCs (Sozen et al., 2019) (Figure S5M). However, this frequency increased when FGF4/TGFβ1 were removed from the medium (45.5% versus 28.6% for CDX2 and 73.2% versus 50.8% for KRT8/18, see

method details) (Figures 5I, 5J, S5M, and S5N). We concluded that the absence of these molecules leaves the blastoid EPI-like cells as the main source of positional information, which facilitates mural differentiation. Accordingly, when exposed to TXV molecules, blastocysts maintained ELF5 and LY6A expression in the mural cells, which were less able to become KRT8/18^{high} (Figures 5K and S5O). Collectively, these data indicate that EPI inducers act locally to pattern the TE axis.

Proximity to inducers maintains the trophectoderm decidualization capacity

After the initial attachment (∼E4.5–5.0), the blastocyst instructs the uterus to form an enveloping decidual tissue (∼E5.0–7.5) but the contribution from different pools of TRs is unknown. Previous experiments showed that trophospheres are composed of differentiated TRs and have a diminished potential to induce decidualization (Gardner and Johnson, 1972; Rossant and Tamura-Lis, 1981; Rivron et al., 2018). Here, we examined whether the polar TE might be critical for decidua formation. To minimize signaling between conceptus and uterus, we first used fixed blastoids. They were incapable of inducing decidua formation (Figures 6A and 6B, p < 0.0001). Along with the diminished potential of trophospheres to decidualize the uterus (Rivron et al., 2018), this suggests that blastoids actively instruct decidualization. Blastoids formed with TESCs or with TSCs including a CDX2 inducible transgene (CDX2i-TSCs, Figure S6A) had an enhanced capacity for decidualization as compared to TSCs blastoids (Figures 6C and 6D, 18.7% versus 7.6%, p = 0.0002; Figure 6F, p = 0.0128). They formed larger deciduae similar in size to that of the blastocyst (Figure 6E) and achieved a higher receptivity rate (Figure S6B, 96.7% versus 64.9%). We concluded that inducers contribute in making the TE competent for decidualization. Blastoids formed from ESCs also had a higher potential to regulate decidualization as compared to blastoids formed from EPSCs (Figure 6E). Finally, a GW501516 treatment of blastoids reduced CDX2 expression and diminished their potential for decidualization (Figures 6G, 6H, and S6C). Overall, we concluded that EPI inducers regulate CDX2 expression, which endows TRs with the capacity to decidualize the uterine tissues, consistent with CDX2 genetic loss-of-function experiments in which null blastocysts fail to implant (Strumpf et al., 2005).

Figure 4. TXV TSCs have an enhanced capacity to self-renew, a lessened propensity to spontaneously differentiate, and a maintained potential to contribute to development

(A) Fluorescence-activated cell sorting (FACS) analysis of cell-cycle profiles of cells cultured in TX and TXV medium based on DNA content measured using Hoechst 34580.

(B) Colony formation efficiency of single sorted TX and TXV TSCs based on three independent experiments and a total 288 wells of cells for each condition.

(C) Ratio of CDX2/EOMES double-positive cells within outgrowths from C57BL/6J mouse blastocysts.

(D and E) Immunostaining against KRT18 and KRT8 (D) and quantification of KRT18- or KRT8-positive cells (E) in TX and TXV TSCs and in TXV TSCs treated with GW501516.

(F) LY6A and KRT18 expression in the E4.5 blastocysts. LY6A was enriched in the polar TE compared to the mural TE and shows clear contrast to KRT18.

(G and H) Immunostaining (G) and flow cytometry (H) analysis for LY6A of TX and TXV TSCs.

(I) Differentiation dynamics of TXV TSCs upon removal of optimal inducers. A sample was taken every 24 h for 6 days after compound removal at t0.

(J) Schematic view for the cell types in E3.5 blastocyst and their derivatives in E7.5 conceptus.

(K) Immunostaining against GFP and ELF5 in E7.5 chimeric embryos obtained upon the injection of blastocysts with serum-cultured TSCs, TX-cultured TSCs, and TXV-cultured TSCs. Non-injected Ctrl represents E7.5 conceptus, which developed from blastocysts that were not injected with TSCs but that, similar to injected blastocysts, underwent laser incision of the Zona Pellucida.

For each graph, data are means ± SEM, analyzed by Student's t test: **p < 0.01, ***p < 0.001. Scale bars: 40 μm in (D); 150 μm in (F) and (G); 300 μm in (K). See also Figure S4.
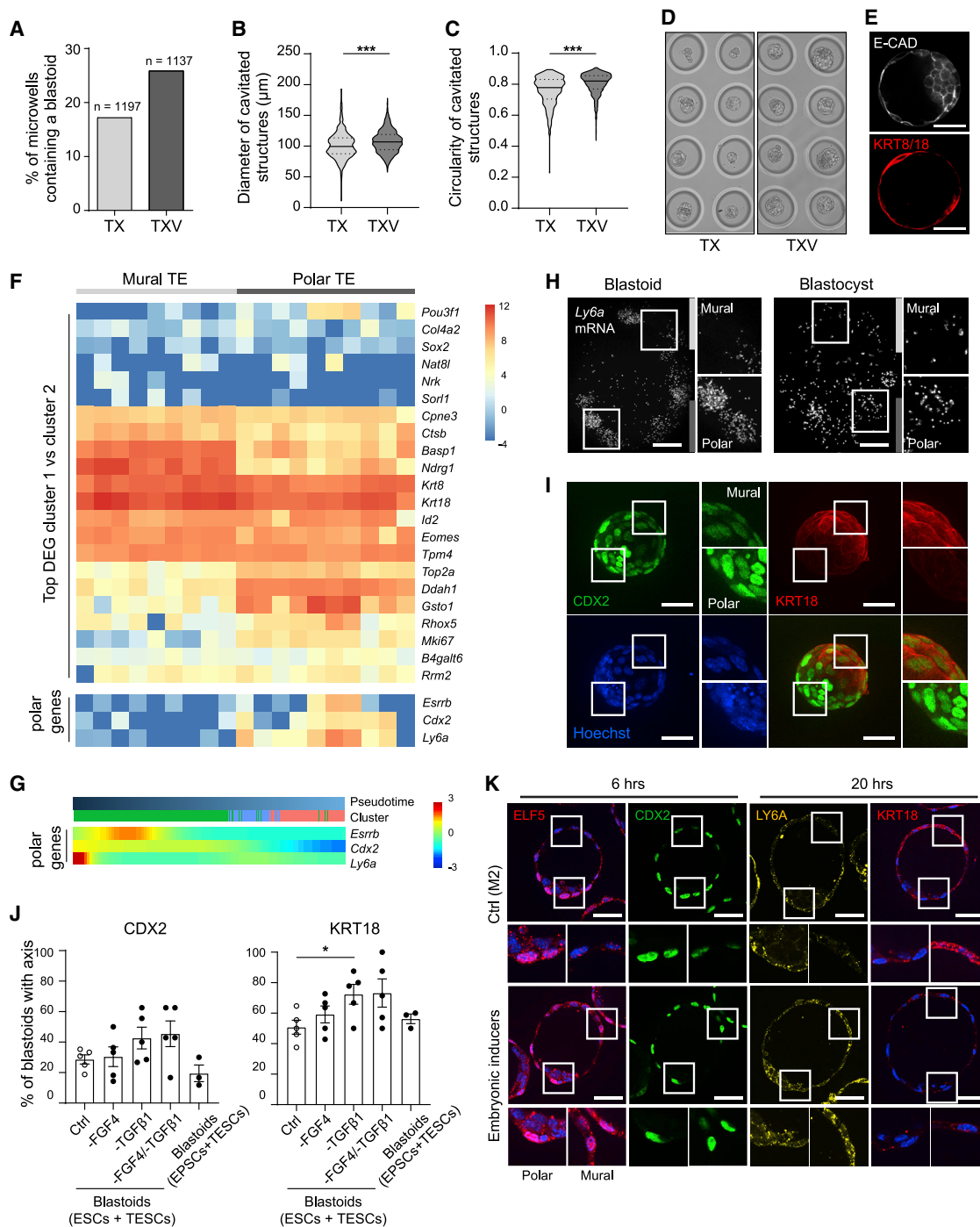
Figure 5. Embryonic inducers pattern the embryonic-abembryonic axis

(A) Percentage of microwells containing a blastoid (based on circularity, diameter, and presence of one single cavity).

(B and C) Diameter (B) and circularity (C) of all structures formed in all microwells for TSCs cultured in TX or TXV medium.

(D) Representative images of microwells containing TX and TXV blastoids.

(E) Blastoid formed from TXV TSCs stained for E-CAD and KRT8/18. Scale bars, 40 μm.

(F) The top differentially expressed genes when comparing clusters 1 and 2 (see Figure S5K) were plotted for the single cells obtained from polar and mural TE from Nakamura et al. (2015). Each column indicates a single cell from the respective group.

(G) Pseudotime heatmap for the polar genes *Esrrb* and *Cdx2* and *Ly6a* (see also Figures S5J and S5K).

(H) smFISH staining for *Ly6a* in a blastoid and blastocyst. Scale bars, 20 μm.

(legend continued on next page)
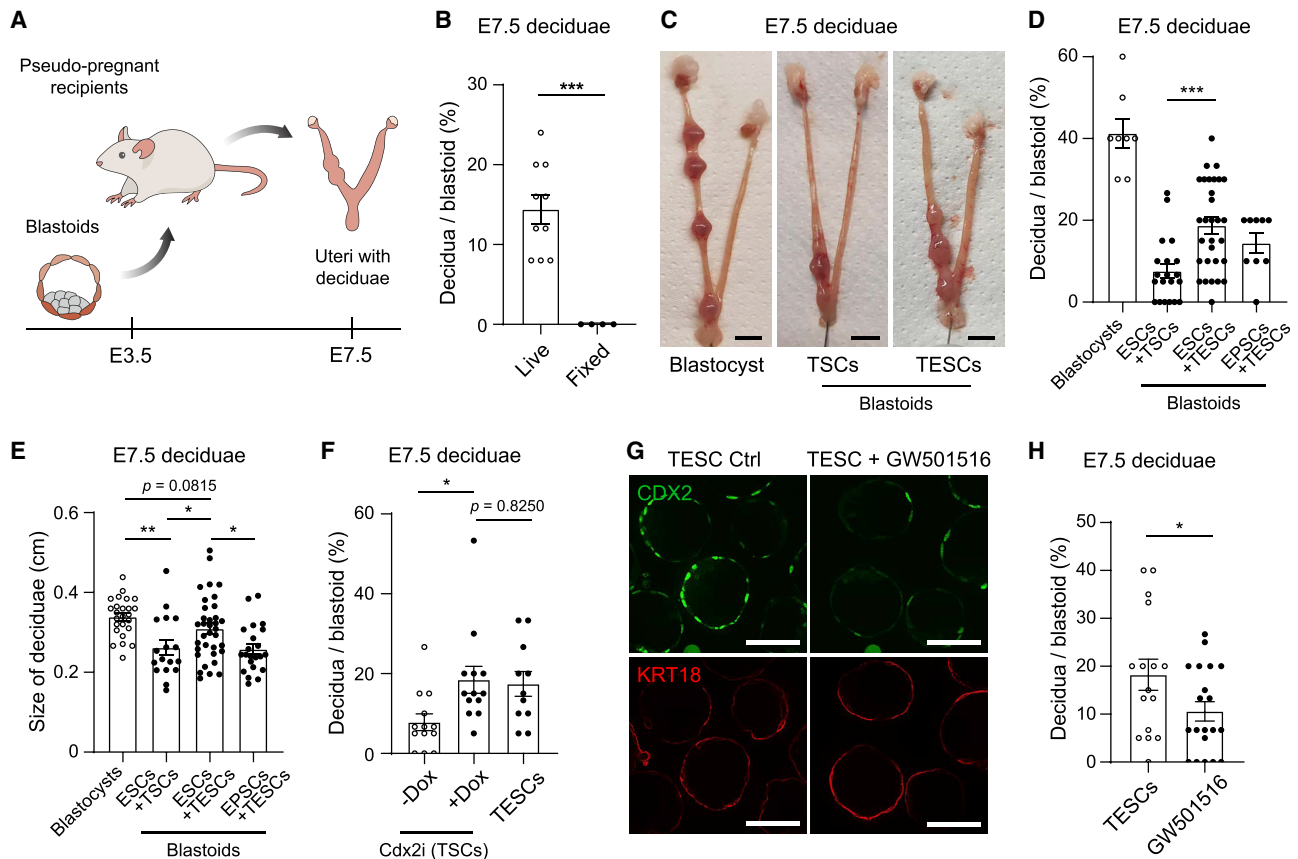
Figure 6. Embryonic inducers capacitate TRs for decidualization

(A) Timeline for uterus transfer and deciduae recovery.

(B) Decidua formation efficiency of live and fixed (dead) blastoids at E7.5. Fixed blastoids were chosen as a negative control instead of concanavalin A (ConA)-coated beads or sesame oil since the latter two have been reported to induce a uterine reaction by physical or signaling interactions (Cuatrecasas and Tell, 1973).

(C) E7.5 deciduae induced by blastocysts, TSCs blastoids, and TESCs blastoids.

(D) Quantification of the implantation efficiency.

(E) Quantification of the size of E7.5 decidua.

(F) Decidua formation efficiency of blastoids formed from CDX2 overexpression inducible TSCs (CDX2i) ± doxycycline (Dox) treatment.

(G) Immunostaining of blastoids formed from GW501516-treated TESCs showed reduced CDX2 expression as well as increased KRT18 expression.

(H) Quantification of the decidua formation efficiency at E7.5.

For (B), (D), (F), and (H), each dot represents an individual mouse. In (C)–(E), each dot represents one decidua. For each graph, data are means ± SEM, analyzed by Student's t test: *p < 0.05, **p < 0.01, ***p < 0.001. Scale bars: 0.5 cm in (C); 100 μm in (G). See also Figure S6.

WNT6/7B are downstream effectors of CDX2 contributing to decidualization

We sought to identify molecules (1) whose secretion is regulated by CDX2 and (2) that could contribute to decidualization. Using the computational framework SCENIC (Aibar et al., 2017), we identified multiple Wnt ligands (*Wnt6* and *Wnt7b*) and receptors (*Fzd2/7/10*) with promoter regions predicted to be bound by CDX2 (two interaction sites for *Wnt6*, one for *Wnt7b* promoter region; Figure 7A). In blastocysts, *Wnt7b* transcripts are the most abundant, followed by *Wnt6*. In addition, *Wnt7b* transcripts are

enriched in CDX2^{high} relative to CDX2^{low} TSCs and upon *Cdx2* overexpression (Figure S7A). Consistent with a role for Wnt in decidualization (Mohamed et al., 2005), WNT7B is highly expressed in the TE and its derivatives (Figure 7B), and *Wnt6/7b* expression is maintained in the ExE (Figure S7B). This expression pattern is conserved in humans with *Wnt6/7b* transcripts being also abundant in the TE (Figure S7C) (). Consistent with a role for TE-secreted Wnt ligands in decidualization, 8-cell embryos cultured with porcupine inhibitor (IWP2, 2.5 μM, 48 h) formed blastocysts that had a significantly decreased potential for decidualization

---

(I) Immunostaining for CDX2 and KRT18 as marker proteins for axis formation in the blastoid. Shown is a representative 3D projection of a TESCs blastoid formed without addition of TGFβ1. Scale bar represents 50 μm.

(J) Percentage of blastoids with an axis for CDX2 or KRT18. Plotted are the mean percentages of five individual experiments (total 40–60 blastoids per group).

(K) Immunostaining of blastocysts cultured with TXV factors for 6 or 20 h. Scale bar, 40 μm.

For each graph, data are means ± SEM, analyzed by Student's t test and one-way ANOVA: *p < 0.05, **p < 0.01, ***p < 0.001. See also Figure S5.
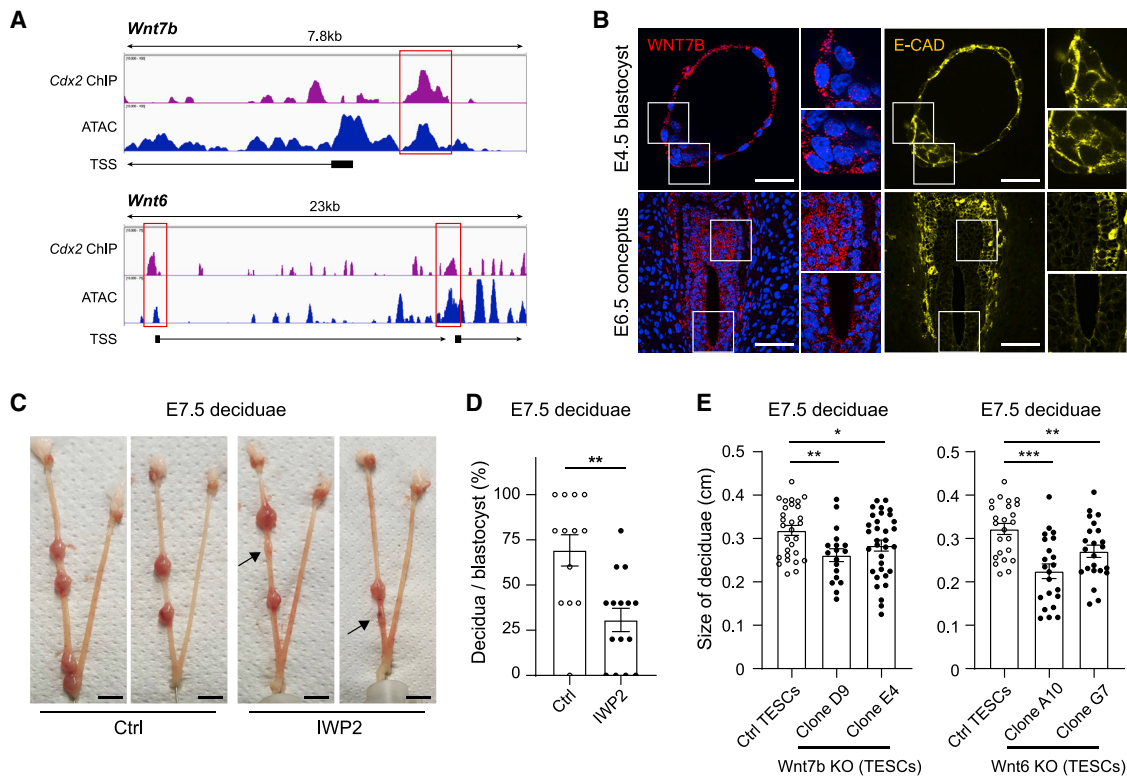
Figure 7. Decidualization by TRs proceeds partly through CDX2 and the secretion of WNT6/7B

(A) CDX2 ChIP-seq analysis of *Wnt7b* and *Wnt6* genes. Peaks in Assay for Transposase-Accessible Chromatin using sequencing (ATAC) show chromatin accessibility. TSS, transcription start site.

(B) Immunostaining of an E4.5 blastocyst and an E6.5 conceptus for WNT7B and E-CAD. WNT7B was detected in the TE rather than the EPI at E4.5. In the E6.5 conceptus, E-CAD$^+$ cells surrounded WNT7B$^+$ cells, reminiscent of the CDX2 and KRT18 expression pattern (Figure 1E). The data indicate that WNT7B is enriched in polar TE derivatives.

(C and D) E7.5 deciduae induced by IWP2-treated blastocysts (C) and quantification of the implantation efficiency (D). Arrows indicate resolving deciduae. Each dot represents an individual mouse.

(E) Quantification of the size of E7.5 decidua from *Wnt7b* KO blastoids (left) and *Wnt6* KO blastoids (right). Each dot represents one decidua.

For each graph, data are means ± SEM, analyzed by Student's t test: *p < 0.05, **p < 0.01, ***p < 0.001. Scale bars: 40 and 80 μm in (B) top and bottom, respectively; 0.5 cm in (C). See also Figure S7.

(Figures 7C and 7D). Many deciduae were immature or resorbed (Figure 7C, arrow). To first model the autocrine functions of Wnt ligands specifically in the TE, we formed trophospheres with *Wnt6* or *Wnt7b* knockout (KO) TESCs (Figures S7D–S7F) (Meistermann et al., 2021). Consistent with a role for WNT activity in TE formation (Rivron et al., 2018), these trophospheres had a decreased cavitation capacity (Figure S7G). This suggests an autocrine function for WNT/7B in TE morphogenesis. Of note, Wnt controls Hippo pathway activity in several other systems. Finally, we observed that blastoids formed with *Wnt6* or *Wnt7b* KO TESCs initially attached to the uterus comparably to wild type (E5.5, Figures S7H and S7I). Thus we did not detect an early attachment defect, often associated with mural TE functions. However, later (E7.5), the diameter of the deciduae was significantly decreased (Figures 7E and S7J). Note that a 20% decrease in sphere diameter correspond to a 2-fold decrease in volume. Taken together, we concluded that the EPI inducers not only locally maintain the TR progenitors, but also support the secretion of Wnt ligands for decidua formation.

DISCUSSION

For development to occur, embryos must maintain progenitors that fuel growth while allowing a subset of cells to differentiate in order to fulfill functions. Here, we show that a specific combination of EPI inductions increases the optimality of the TF network (CDX2, EOMES, and ESRRB), enhances self-renewal, and prevents differentiation. On the contrary, suboptimal exposure to inducers favors a fluctuation of the progenitor state, creating reversible subpopulations with facilitated differentiation. We propose that the dynamic regulation of this EPI/TR interface endows the progenitor pool with a flexible strategy for either maintaining more progenitors or generating differentiated cell types. We surmise that cellular heterogeneity arises as the embryo exploits a suboptimal environment to control an equilibrium between interconvertible TR populations. This EPI/TR interface and the reversibility of cellular states would endow the progenitor pool with adaptive and regulative properties to synchronize tissue development, thus acting as a checkpoint.

Conceivably, the rapid geometric changes (size and shape) of the developing embryo influence the exposure to EPI inducers, thus linking morphogenesis with the maintenance of TR progenitors.

The origin of the observed heterogeneity and plasticity of TSCs is unknown. Upstream CDX2 regulators (e.g., Hippo/Notch signaling components) can vary stochastically (Sigal et al., 2006) due to the properties of intracellular biochemical loops or to fluctuations in cell-cell membrane interactions. CDX2 expression might also be regulated by geometrical or mechanical cues as observed during the morula-to-blastocyst transition. Beyond inductions, both the intrinsic properties of biochemical networks and extrinsic geometric cues might thus contribute to distributing cell states. Signaling pathways act as CDX2 regulators but also as inducers of histone remodeling. For example, Notch activates target genes with trimethylation of H3K4 by inhibiting dimethyl-transferase (KDM5A) activity (Rayon et al., 2014; (Liefke et al., 2010)). Hippo signaling also controls histone remodeling (Hillmer and Link, 2019). Our data showed higher trimethylation of H3K4 (H3K4me3) in CDX2^{high} cells. Thus, in the CDX2^{low} TRs that are prone to differentiation, epigenetic mechanisms might act as feedforward loops engraving the differentiation path.

Blastoids formed from TESCs spontaneously generate a gene expression pattern along the axis. We conclude from these experiments of reconstruction that, following subtle early patterning events (Graham and Zernicka-Goetz, 2016; Zhang and Hiiragi, 2018), the EPI produces inductive signals that significantly contribute to axis formation. This process ultimately ensures the blastocyst/uterus interaction of implantation. We propose that inducers, including LPA, FGF4, Nodal, BMP4, BMP7, and IL6/11, contribute toward regulating CDX2 expression in the polar TE, which impacts proliferation, self-renewal, and epithelial morphogenesis but also the expression of WNT ligands that contribute to decidualization. The regulation of WNT ligands might be a mechanism with potential translational applicability to human implantation (Koler et al., 2009).

Altogether, this study provides a framework to explain how the conceptus leverages inductions and TR state fluctuation to maintain progenitors, facilitate differentiation, or allocate and balance the functions necessary for implantation to occur.

Limitation of study

Although blastoids formed with ESCs and TESCs implant better into the uterus and form decidua more efficiently than blastoids formed with ESCs and TSCs, we did not observe the formation of a fetus. The minimal requirements for development to occur are not yet met.

We selected WNT6 and WNT7b as downstream effectors of CDX2 based on RNA-seq, ChIP, TESC and CDX2 overexpression analysis in TSCs, and the expression pattern of these genes in the TE of human blastocysts. We propose that these WNT ligands follow the dynamical expression pattern of CDX2. However, decidualization is a complex process that involves multiple players. Beyond WNT6/7b, other molecules secreted by the conceptus might affect decidualization.

STAR★METHODS

Detailed methods are provided in the online version of this paper and include the following:

- KEY RESOURCES TABLE
- RESOURCE AVAILABILITY
  - Lead contact
  - Material availability
  - Data and code availability
- EXPERIMENTAL MODEL AND SUBJECT DETAILS
  - Stem cells and culture condition
  - Mouse lines and embryos
- METHOD DETAILS
  - Generation of inducible Caudal Type Homeobox 2 overexpression cell lines
  - Generation of WNT6 and WNT7B knockout trophoblast stem cells
  - Cell cycle analysis
  - Colony formation assay
  - Combinatorial screen
  - Immunofluorescence
  - Whole tissue staining/clearing and 3D imaging of embryos
  - Single-molecule FISH
  - Single-molecule FISH polarity quantification
  - High content imaging
  - Live cell imaging
  - Flow cytometry
  - qRT-PCR
  - RNA sequencing
  - Mapping and processing of single-cell mRNA sequencing data
  - Analysis of single-cell mRNA sequencing data
  - Caudal Type Homeobox 2 ChIP-seq analysis
  - Chromatin immunoprecipitation PCR (ChIP-PCR)
  - Chimeric embryo formation
  - Trophoblast stem cells line derivation and staining
  - Blastoid formation
  - Uterus transfer and decidua analysis
  - Blue band assay
  - Western Blot
  - SCOPE and PTUI
- QUANTIFICATION AND STATISTICAL ANALYSIS

AUTHOR CONTRIBUTIONS

DECLARATION OF INTERESTS

INCLUSION AND DIVERSITY

REFERENCES

Aibar, S., Gonzalez-Blas, C.B., Moerman, T., Huynh-Thu, V.A., Imrichova, H., Hulselmans, G., Rambow, F., Marine, J.C., Geurts, P., Aerts, J., et al. (2017). SCENIC: single-cell regulatory network inference and clustering. Nat. Methods *14*, 1083–1086. https://doi.org/10.1038/nmeth.4463.

Aubin, J., Davy, A., and Soriano, P. (2004). In vivo convergence of BMP and MAPK signaling pathways: impact of differential Smad1 phosphorylation on development and homeostasis. Genes Development *18*, 1482–1494. https://doi.org/10.1101/gad.1202604.

Auman, H.J., Nottoli, T., Lakiza, O., Winger, Q., Donaldson, S., and Williams, T. (2002). Transcription factor AP-2γ is essential in the extra-embryonic lineages for early postimplantation development. Development *129*, 2733–2747. https://doi.org/10.1242/dev.129.11.2733.

Azami, T., Bassalert, C., Allègre, N., Valverde Estrella, L., Pouchin, P., Ema, M., and Chazaud, C. (2019). Regulation of the ERK signalling pathway in the developing mouse blastocyst. Development *146*, dev177139.

Barrientos, G., Freitag, N., Tirado-Gonzalez, I., Unverdorben, L., Jeschke, U., Thijssen, V.L., and Blois, S.M. (2014). Involvement of galectin-1 in reproduction: past, present and future. Hum. Reprod. Update *20*, 175–193. https://doi.org/10.1093/humupd/dmt040.

Ben-Haim, N., Lu, C., Guzman-Ayala, M., Pescatore, L., Mesnard, D., Bischofberger, M., Naef, F., Robertson, E., and Constam, D.B. (2006). The nodal precursor acting via activin receptors induces mesoderm by maintaining a source of its convertases and BMP4. Dev. Cell *11*, 313–323. https://doi.org/10.1016/j.devcel.2006.07.005.

Cha, J., Sun, X., and Dey, S.K. (2012). Mechanisms of implantation: strategies for successful pregnancy. Nature Medicine *18*, 1754–1767. https://doi.org/10.1038/nm.3012.

Chai, N., Patel, Y., Jacobson, K., McMahon, J., McMahon, A., and Rappolee, D.A. (1998). FGF is an essential regulator of the fifth cell division in preimplantation mouse embryos. Developmental Biology *198*, 105–115.

Chambers, I., Silva, J., Colby, D., Nichols, J., Nijmeijer, B., Robertson, M., Vrana, J., Jones, K., Grotewold, L., and Smith, A. (2007). Nanog safeguards pluripotency and mediates germline development. Nature *450*, 1230–1234. https://doi.org/10.1038/nature06403.

Constam, D.B., and Robertson, E.J. (2000). SPC4/PACE4 regulates a TGFβ signaling network during axis formation. Genes Development *14*, 1146–1155. https://doi.org/10.1101/gad.14.9.1146.

Constância, M., Hemberger, M., Hughes, J., Dean, W., Ferguson-Smith, A., Fundele, R., Stewart, F., Kelsey, G., Fowden, A., Sibley, C., and Reik, W. (2002). Placental-specific IGF-II is a major modulator of placental and fetal growth. Nature *417*, 945–948. https://doi.org/10.1038/nature00819.

Copp, A.J. (1978). Interaction between inner cell mass and trophectoderm of the mouse blastocyst. J. Embryol. Exp. Morphol. *48*, 109–125. https://doi.org/10.1242/dev.48.1.109.

Corson, L.B., Yamanaka, Y., Lai, K.M.V., and Rossant, J. (2003). Spatial and temporal patterns of ERK signaling during mouse embryogenesis. Development *130*, 4527–4537. https://doi.org/10.1242/dev.00669.

Cuatrecasas, P., and Tell, G.P.E. (1973). Insulin-like activity of concanavalin A and wheat germ agglutinin–direct interactions with insulin receptors. Proceedings of the National Academy of Sciences of the United States of America *70*, 485–489. https://doi.org/10.1073/pnas.70.2.485.

Das, S.K., Wang, X., Paria, B., Damm, D., Abraham, J., Klagsbrun, M., Andrews, G., and Dey, S. (1994). Heparin-binding EGF-like growth factor gene is induced in the mouse uterus temporally by the blastocyst solely at the site of its apposition: a possible ligand for interaction with blastocyst EGF-receptor in implantation. Development *120*, 1071–1083. https://doi.org/10.1242/dev.120.5.1071.

Donnison, M., Beaton, A., Davey, H.W., Broadhurst, R., L'Huillier, P., and Pfeffer, P.L. (2005). Loss of the extraembryonic ectoderm in Elf5 mutants leads to defects in embryonic patterning. Development *132*, 2299–2308. https://doi.org/10.1242/dev.01819.

Ema, M., Mori, D., Niwa, H., Hasegawa, Y., Yamanaka, Y., Hitoshi, S., Mimura, J., Kawabe, Y., Hosoya, T., Morita, M., et al. (2008). Krüppel-like factor 5 is essential for blastocyst development and the normal self-renewal of mouse ESCs. Cell Stem Cell *3*, 555–567. https://doi.org/10.1016/j.stem.2008.09.003.

Frias-Aldeguer, J., Kip, M., Vivié, J., Li, L., Alemany, A., Korving, J., Darmis, F., van Oudenaarden, A., Geijsen, N., and Rivron, N.C. (2020). Embryonic signals perpetuate polar-like trophoblast stem cells and pattern the blastocyst axis. Preprint at bioRxiv. https://doi.org/10.1101/510362.

Fujii, H., Tatsumi, K., Kosaka, K., Yoshioka, S., Fujiwara, H., and Fujii, S. (2006). Eph-ephrin A system regulates murine blastocyst attachment and spreading. Dev. Dynam. *235*, 3250–3258.

Gao, H., Gao, R., Zhang, L., Xiu, W., Zang, R., Wang, H., Zhang, Y., Chen, J., Gao, Y., and Gao, S. (2018). Esrrb plays important roles in maintaining self-renewal of trophoblast stem cells (TSCs) and reprogramming somatic cells to induced TSCs. J. Mol. Cell Biol. *11*, 463–473. [Preprint]. https://doi.org/10.1093/jmcb/mjy054.

Gardner, R.L. (1983). Origin and differentiation of extraembryonic tissues in the mouse. Int. Rev. Exp. Pathol. *24*, 63–133.

Gardner, R.L. (2000). Flow of cells from polar to mural trophectoderm is polarized in the mouse blastocyst. Human Reproduction *15*, 694–701. https://doi.org/10.1093/humrep/15.3.694.

Gardner, R.L., and Johnson, M.H. (1972). An investigation of inner cell mass and trophoblast tissues following their isolation from the mouse blastocyst. J. Embryol. Exp. Morphol. *28*, 279–312. https://doi.org/10.1242/dev.28.2.279.

Gardner, R.L., Papaioannou, V.E., and Barton, S.C. (1973). Origin of the ectoplacental cone and secondary giant cells in mouse blastocysts reconstituted

transcriptomes reveals the dynamics of lineage specification. Cell Stem Cell *28*, 1625–1640.e6.

Mesnard, D., Donnison, M., Fuerer, C., Pfeffer, P.L., and Constam, D.B. (2011). The microenvironment patterns the pluripotent mouse epiblast through paracrine Furin and Pace4 proteolytic activities. Genes Development *25*, 1871–1880. https://doi.org/10.1101/gad.16738711.

Miura, S., Singh, A.P., and Mishina, Y. (2010). Bmpr1a is required for proper migration of the AVE through regulation of Dkk1 expression in the pre-streak mouse embryo. Developmental Biology *341*, 246–254. https://doi.org/10.1016/j.ydbio.2010.02.038.

Mohamed, O.A., Jonnaert, M., Labelle-Dumais, C., Kuroda, K., Clarke, H.J., and Dufort, D. (2005). Uterine Wnt/β-catenin signaling is required for implantation. Proceedings of the National Academy of Sciences of the United States of America *102*, 8579–8584. https://doi.org/10.1073/pnas.0500612102.

Moriwaki, K., Tsukita, S., and Furuse, M. (2007). Tight junctions containing claudin 4 and 6 are essential for blastocyst formation in preimplantation mouse embryos. Developmental Biology *312*, 509–522. https://doi.org/10.1016/j.ydbio.2007.09.049.

Motomura, K., Oikawa, M., Hirose, M., Honda, A., Togayachi, S., Miyoshi, H., Ohinata, Y., Sugimoto, M., Abe, K., Inoue, K., and Ogura, A. (2016). Cellular dynamics of mouse trophoblast stem cells: Identification of a persistent stem cell type. Biol. Reprod. *94*, 122. https://doi.org/10.1095/biolreprod.115.137125.

Murohashi, M., Nakamura, T., Tanaka, S., Ichise, T., Yoshida, N., Yamamoto, T., Shibuya, M., Schlessinger, J., and Gotoh, N. (2010). An FGF4-FRS2α-Cdx2 Axis in trophoblast stem cells induces Bmp4 to regulate proper growth of early mouse embryos. Stem Cells *28*, 113–121. https://doi.org/10.1002/stem.247.

Nakamura, T., Yabuta, Y., Okamoto, I., Aramaki, S., Yokobayashi, S., Kurimoto, K., Sekiguchi, K., Nakagawa, M., Yamamoto, T., and Saitou, M. (2015). SC3-seq: a method for highly parallel and quantitative measurement of single-cell gene expression. Nucleic Acids Research *43*, e60. https://doi.org/10.1093/nar/gkv134.

Nakao, A., Afrakhte, M., Morn, A., Nakayama, T., Christian, J.L., Heuchel, R., Itoh, S., Kawabata, M., Heldin, N.E., Heldin, C.H., and Dijke, P. (1997). Identification of Smad7, a TGFβ-inducible antagonist of TGF-β signalling. Nature *389*, 631–635. https://doi.org/10.1038/39369.

Natale, B.V., Schweitzer, C., Hughes, M., Globisch, M.A., Kotadia, R., Tremblay, E., Vu, P., Cross, J.C., and Natale, D.R.C. (2017). Sca-1 identifies a trophoblast population with multipotent potential in the mid-gestation mouse placenta. Sci. Rep. *7*, 5575. https://doi.org/10.1038/s41598-017-06008-2.

Nichols, J., and Smith, A. (2012). Pluripotency in the embryo and in culture. Cold Spring Harbor perspectives in biology *4*, a008128.

Nichols, J., Zevnik, B., Anastassiadis, K., Niwa, H., Klewe-Nebenius, D., Chambers, I., Scholer, H., and Smith, A. (1998). Formation of pluripotent stem cells in the mammalian embryo depends on the POU transcription factor Oct4. Cell *95*, 379–391. https://doi.org/10.1016/s0092-8674(00)81769-9.

Nishioka, N., Yamamoto, S., Kiyonari, H., Sato, H., Sawada, A., Ota, M., Nakao, K., and Sasaki, H. (2008). Tead4 is required for specification of trophectoderm in pre-implantation mouse embryos. Mech. Dev. *125*, 270–283. https://doi.org/10.1016/j.mod.2007.11.002.

Nishioka, N., Inoue, K., Adachi, K., Kiyonari, H., Ota, M., Ralston, A., Yabuta, N., Hirahara, S., Stephenson, R.O., Ogonuki, N., et al. (2009). The Hippo signaling pathway components Lats and Yap pattern Tead4 activity to distinguish mouse trophectoderm from inner cell mass. Dev. Cell *16*, 398–410. https://doi.org/10.1016/j.devcel.2009.02.003.

Ohinata, Y., and Tsukiyama, T. (2014). Establishment of trophoblast stem cells under defined culture conditions in mice. PLoS One *9*, e107308. https://doi.org/10.1371/journal.pone.0107308.

Ohnishi, Y., Huber, W., Tsumura, A., Kang, M., Xenopoulos, P., Kurimoto, K., Oles, A.K., Arauzo-Bravo, M.J., Saitou, M., Hadjantonakis, A.K., and Hiiragi, T. (2014). Cell-to-cell expression variability followed by signal reinforcement progressively segregates early mouse lineages. Nat. Cell Biol. *16*, 27–37. https://doi.org/10.1038/ncb2881.

Perez-Garcia, V., Lea, G., Lopez-Jimenez, P., Okkenhaug, H., Burton, G.J., Moffett, A., Turco, M.Y., and Hemberger, M. (2021). BAP1/ASXL complex

modulation regulates epithelial-mesenchymal transition during trophoblast differentiation and invasion. Elife *10*. https://doi.org/10.7554/eLife.63254.

Posfai, E., Schell, J.P., Janiszewski, A., Rovic, I., Murray, A., Bradshaw, B., Yamakawa, T., Pardon, T., El Bakkali, M., Talon, I., et al. (2021). Evaluating totipotency using criteria of increasing stringency. Nat. Cell Biol. *23*, 49–60. https://doi.org/10.1038/s41556-020-00609-2.

Rayon, T., Menchero, S., Nieto, A., Xenopoulos, P., Crespo, M., Cockburn, K., Canon, S., Sasaki, H., Hadjantonakis, A.K., de la Pompa, J., et al. (2014). Notch and hippo converge on Cdx2 to specify the trophectoderm lineage in the mouse blastocyst. Dev. Cell *30*, 410–422. https://doi.org/10.1016/j.devcel.2014.06.019.

Rhee, C., Lee, B.K., Beck, S., LeBlanc, L., Tucker, H.O., and Kim, J. (2017). Mechanisms of transcription factor-mediated direct reprogramming of mouse embryonic stem cells to trophoblast stem-like cells. Nucleic acids research *45*, 10103–10114.

Rivron, N.C., Frias-Aldeguer, J., Vrij, E.J., Boisset, J.C., Korving, J., Vivie, J., Truckenmuller, R.K., van Oudenaarden, A., van Blitterswijk, C.A., and Geijsen, N. (2018). Blastocyst-like structures generated solely from stem cells. Nature *557*, 106–111. https://doi.org/10.1038/s41586-018-0051-0.

Roebroek, A.J., Umans, L., Pauli, I., Robertson, E., van Leuven, F., Van de Ven, W., and Constam, D. (1998). Failure of ventral closure and axial rotation in embryos lacking the proprotein convertase Furin. Development *125*, 4863–4876. https://doi.org/10.1242/dev.125.24.4863.

Rossant, J., and Tamura-Lis, W. (1981). Effect of culture conditions on diploid to giant-cell transformation in postimplantation mouse trophoblast. J. Embryol. Exp. Morphol. *62*, 217–227. https://doi.org/10.1242/dev.62.1.217.

Rugg-Gunn, P.J., Cox, B.J., Ralston, A., and Rossant, J. (2010). Distinct histone modifications in stem cell lines and tissue lineages from the early mouse embryo. Proceedings of the National Academy of Sciences of the United States of America *107*, 10783–10790. https://doi.org/10.1073/pnas.0914507107.

Saba-El-Leil, M.K., Vella, F.D., Vernay, B., Voisin, L., Chen, L., Labrecque, N., Ang, S.L., and Meloche, S. (2003). An essential function of the mitogen-activated protein kinase Erk2 in mouse trophoblast development. EMBO Rep *4*, 964–968.

Sebastiano, V., Dalvai, M., Gentile, L., Schubart, K., Sutter, J., Wu, G.M., Tapia, N., Esch, D., Ju, J.Y., Hubner, K., et al. (2010). Oct1 regulates trophoblast development during early mouse embryogenesis. Development *137*, 3551–3560. https://doi.org/10.1242/dev.047027.

Seong, J., Kim, N.S., Kim, J.A., Lee, W., Seo, J.Y., Yum, M.K., Kim, J.H., Park, I., Kang, J.S., Bae, S.H., et al. (2018). Side branching and luminal lineage commitment by ID2 in developing mammary glands. Development *145*. https://doi.org/10.1242/dev.165258.

Shindo, T., Manabe, I., Fukushima, Y., Tobe, K., Aizawa, K., Miyamoto, S., Kawai-Kowase, K., Moriyama, N., Imai, Y., Kawakami, H., et al. (2002). Krüppel-like zinc-finger transcription factor KLF5/BTEB2 is a target for angiotensin II signaling and an essential regulator of cardiovascular remodeling. Nat. Med. *8*, 856–863. https://doi.org/10.1038/nm738.

Shi, X.-H., Larkin, J.C., Chen, B., and Sadovsky, Y. (2013). The expression and localization of N-myc downstream-regulated gene 1 in human trophoblasts. PLoS One *8*, e75473. https://doi.org/10.1371/journal.pone.0075473.

Sigal, A., Milo, R., Cohen, A., Geva-Zatorsky, N., Klein, Y., Liron, Y., Rosenfeld, N., Danon, T., Perzov, N., and Alon, U. (2006). Variability and memory of protein levels in human cells. Nature *444*, 643–646. https://doi.org/10.1038/nature05316.

Sood, R., Zehnder, J.L., Druzin, M.L., and Brown, P.O. (2006). Gene expression patterns in human placenta. Proceedings of the National Academy of Sciences of the United States of America *103*, 5478–5483. https://doi.org/10.1073/pnas.0508035103.

Sozen, B., Cox, A.L., De Jonghe, J., Bao, M., Hollfelder, F., Glover, D.M., and Zernicka-Goetz, M. (2019). Self-organization of mouse stem cells into an Extended potential blastoid. Dev. Cell *51*, 698–712.e8. e8.

Strumpf, D., Mao, C.A., Yamanaka, Y., Ralston, A., Chawengsaksophak, K., Beck, F., and Rossant, J. (2005). Cdx2 is required for correct cell fate

specification and differentiation of trophectoderm in the mouse blastocyst. Development *132*, 2093–2102. https://doi.org/10.1242/dev.01801.

Sutherland, A. (2003). Mechanisms of implantation in the mouse: differentiation and functional importance of trophoblast giant cell behavior. Developmental Biology *258*, 241–251. https://doi.org/10.1016/s0012-1606(03)00130-1.

Tanaka, S., Kunath, T., Hadjantonakis, A.K., Nagy, A., and Rossant, J. (1998). Promotion of trophoblast stem cell proliferation by FGF4. Science *282*, 2072–2075. https://doi.org/10.1126/science.282.5396.2072.

Trapnell, C., Cacchiarelli, D., Grimsby, J., Pokharel, P., Li, S., Morse, M., Lennon, N.J., Livak, K.J., Mikkelsen, T.S., and Rinn, J.L. (2014). The dynamics and regulators of cell fate decisions are revealed by pseudotemporal ordering of single cells. Nat. Biotechnol. *32*, 381–386. https://doi.org/10.1038/nbt.2859.

Tsuji, A., Sakurai, K., Kiyokage, E., Yamazaki, T., Koide, S., Toida, K., Ishimura, K., and Matsuda, Y. (2003). Secretory proprotein convertases PACE4 and PC6A are heparin-binding proteins which are localized in the extracellular matrix. Potential role of PACE4 in the activation of proproteins in the extracellular matrix' Biochimica et biophysica acta *1645*, 95–104. https://doi.org/10.1016/s1570-9639(02)00532-0.

Ueno, M., Lee, L., Chhabra, A., Kim, Y., Sasidharan, R., Van Handel, B., Wang, Y., Kamata, M., Kamran, P., Sereti, K.I., et al. (2013). c-Met-dependent multipotent labyrinth trophoblast progenitors establish placental exchange interface. Dev. Cell *27*, 373–386. https://doi.org/10.1016/j.devcel.2013.10.019.

Weinstein, M., Yang, X., Li, C., Xu, X., Gotay, J., and Deng, C.X. (1998). Failure of egg cylinder elongation and mesoderm induction in mouse embryos lacking the tumor suppressor smad2. Proceedings of the National Academy of Sciences of the United States of America *95*, 9378–9383. https://doi.org/10.1073/pnas.95.16.9378.

Werling, U., and Schorle, H. (2002). Transcription factor gene AP-2 gamma essential for early murine development. Molecular and Cellular Biology *22*, 3149–3156. https://doi.org/10.1128/mcb.22.9.3149-3156.2002.

Wu, T., Wang, H., He, J., Kang, L., Jiang, Y., Liu, J., Zhang, Y., Kou, Z., Liu, L., Zhang, X., and Gao, S. (2011). Reprogramming of trophoblast stem cells into pluripotent stem cells by Oct4. Stem Cells *29*, 755–763. https://doi.org/10.1002/stem.617.

Xie, H., Tranguch, S., Jia, X., Zhang, H., Das, S.K., Dey, S.K., Kuo, C.J., and Wang, H. (2008). Inactivation of nuclear Wnt-β-catenin signaling limits blastocyst competency for implantation. Development *135*, 717–727. https://doi.org/10.1242/dev.015339.

Yagi, R., Kohn, M.J., Karavanova, I., Kaneko, K.J., Vullhorst, D., DePamphilis, M.L., and Buonanno, A. (2007). Transcription factor TEAD4 specifies the trophectoderm lineage at the beginning of mammalian development. Development *134*, 3827–3836. https://doi.org/10.1242/dev.010223.

Yang, W., Klaman, L.D., Chen, B., Araki, T., Harada, H., Thomas, S.M., George, E.L., and Neel, B.G. (2006). An Shp2/SFK/Ras/Erk signaling pathway controls trophoblast stem cell Survival. Dev. Cell *10*, 317–327. https://doi.org/10.1016/j.devcel.2006.01.002.

Ying, Q.L., Wray, J., Nichols, J., Batlle-Morera, L., Doble, B., Woodgett, J., Cohen, P., and Smith, A. (2008). The ground state of embryonic stem cell self-renewal. Nature *453*, 519–523.

You, J.-L., Wang, W., Tang, M.Y., Ye, Y.H., Liu, A.X., and Zhu, Y.M. (2018). A potential role of galectin-1 in promoting mouse trophoblast stem cell differentiation. Mol. Cell. Endocrinol. *470*, 228–239. https://doi.org/10.1016/j.mce.2017.11.003.

Yu, B., van Tol, H.T.A., Oei, C.H.Y., Stout, T.A.E., and Roelen, B.A.J. (2021). Lysophosphatidic acid Accelerates Bovine in vitro-produced blastocyst formation through the hippo/YAP pathway. Int. J. Mol. Sci. *22*, 5915. https://doi.org/10.3390/ijms22115915.

Yu, F.-X., Zhao, B., Panupinthu, N., Jewell, J., Lian, I., Wang, L., Zhao, J., Yuan, H., Tumaneng, K., Li, H., et al. (2012). Regulation of the hippo-YAP pathway by G-protein-Coupled receptor signaling. Cell *150*, 780–791. https://doi.org/10.1016/j.cell.2012.06.037.

Zechner, U., Hemberger, M., Constancia, M., Orth, A., Dragatsis, I., Luttges, A., Hameister, H., and Fundele, R. (2002). Proliferation and growth factor expression in abnormally enlarged placentas of mouse interspecific hybrids. an official publication of the American Association of Anatomists *224*, 125–134. https://doi.org/10.1002/dvdy.10094.

Zhang, H.T., and Hiiragi, T. (2018). Symmetry Breaking in the mammalian embryo. Annu. Rev. Cell Dev. Biol. *34*, 405–426. https://doi.org/10.1146/annurev-cellbio-100617-062616.

STAR★METHODS

KEY RESOURCES TABLE

REAGENT or RESOURCE	SOURCE	IDENTIFIER
Antibodies		
anti-CDX2	Abcam	Ab76541; RRID:AB_1523334
anti-CDX2	BioGenex	MU392A-5UC
anti-E-CADHERIN	BD Biosciences	610182; RRID:AB_397581
anti-ELF5	Santa Cruz	sc-9645; RRID:AB_640106
anti-TBR2/EOMES	Abcam	ab23345; RRID:AB_778267
anti-GFP	Abcam	ab13970; RRID:AB_300798
anti-KRT8/18	DAKO	M365201-2
anti-KRT8	Novus Biological	NBP2-44941-0.1mg
anti-KRT18	Thermo Scientific	MA1-06326
anti-LY6A	Abcam	ab51317; RRID:AB_1640946
anti-WNT7B	R&D Systems	AF3460; RRID:AB_2304437
anti-α-TUBULIN	Cell signaling	3873s
Hoechst	Invitrogen	H3570
WGA	Invitrogen	w11261
Bacterial and virus strains		
DH5a	In house	N/A
Chemicals, peptides, and recombinant proteins		
DMEM/F-12	In-house	N/A
L-ascorbic acid 2-phosphate (ASAP)	Sigma	A8960
Gibc Insulin Transferrin Selenium (ITS-G)	Gibco	12097549
GlutaMAX	Gibco	35050038
Sodium Pyruvate	Gibco	11360070
HEPES	In-house	N/A
β-mercaptoethanol	Gibco	31350010
Penicillin/streptomycin	Sigma	P0781
MEM Non-essential amino acid (NEAA)	Gibco	11140035
Human FGF-4	R&D system	235-F4
Human TGF-β1 (HEK293 derived)	PeproTech	100-21
Heparin	Sigma	H3149
Human/Murine/Rat Activin A (CHO derived)	PeproTech	120-14P
Murine IL11	PeproTech	220-11
human BMP7	PeproTech	120-03p
8-Br cAMP	BIOLOG	B 007-500
1-Oleoyl Lysophosphatidic Acid (LPA)	Tocris	2256236
Y-27632	MedChem Express	HY-10583
(Adv.) DMEM/F-12	Gibco	12634010
Neurobasal medium	Gibco	21103049
N-2 supplement	Gibco	17502048
B-27 supplement	Gibco	A1895602
CHIR 99021	MedChem Express	HY-10182
PD 0325901	MedChem Express	HY-10254
LIF (ESGRO)	Merck	ESG1107
BSA (35%)	Sigma	A7409
Doxycyclin	Sigma	D9891
GW501516	MedChem Express	HY-10838

(Continued on next page)

Continued

REAGENT or RESOURCE	SOURCE	IDENTIFIER
Laminin 521	Biolamina	LN521-05
Matrigel, GFR, Phenol red free	Corning	356231
Accutase	BioLegend	423201
TrypLE Express Enzyme (1x), no phenol red	Gibco	12604039
PMSG	Hölzel Diagnostika	OPPA01037
hCG	MSD	Chorulon 1500 IU
Tyrode's acid solution	Sigma	T1788
4-ring dish	Greiner CELLSTAR	627 170
Quickblasto	Janvier Lab	N/A
EmbryoMax M2 medium	Millipore Sigma	MR-015P-D
EmbryoMax KSOM medium	Millipore Sigma	MR-101-D
0.4% Trypan blue	Thermofisher Scientific	T10282
Critical commercial assays		
Quantigene ViewRNA kit	Affymetrix	QVC0001
RNeasy Mini Kit	Quiagen	74104
innuPREP RNA Mini Kit 2.0	Analytik Jena	845-KS-2040050
ChIP-IT High Sensitivity kit	Active Motif	53040 version A6
Deposited data		
Raw and Processed data	This paper	GEO: GSE200961
"Single cell transcriptome analysis of TSCs differentiated TSCs, pTSCs and pTSCs isolated from blastoid"	This paper and (Frias-Aldeguer et al., 2020)	GEO: GSE127754
"SC3-Seq: A Method for Highly Parallel and Quantitative Measurement of Single-Cell Gene Expression"	Nakamura et al., 2015	GEO: GSE63266
"Evaluating Totipotency Using Criteria of Increasing Stringency"	(Posfai et al., 2021)	GEO: GSE145609
"Mechanisms of transcription factor-mediated direct reprogramming of mouse embryonic stem cells to trophoblast stem-like cells"	(Rhee et al., 2017)	GSE90752 (GSM2412032, GSM2412027)
BirA cells_ChIP	Jonghwan Kim	GSM2412036
Codes for RNA-seq analysis	This paper	https://doi.org/10.5281/zenodo.6602725 (https://zenodo.org/record/6602725#.YpdYZqhBxaQ)
Experimental models: Cell lines		
F4-GFP TSCs	Gift obtained from Hospital for Sick Children, Toronto, ON, Canada (J. Rossant lab)	N/A
F4-GFP Cdx2-inducible TSCs	This paper	N/A
CDX2-eGFP TSCs	Gift obtained from Hospital for Sick Children, Toronto, ON, Canada (J. Rossant lab)	N/A
G4 ESCs	Gift obtained from Samuel Lunenfeld Research Institute, Mount Sinai Hospital, Toronto, ON, Canada (A. Nagy lab)	N/A
H2B-RFP ESCs	Gift obtained from the Whitehead Institute for Biomedical Research and Department of Biology, MIT, Cambridge (R. Jaenisch lab)	N/A
Experimental models: Organisms/strains		
Mouse_C57BL/6J	The Jackson Laboratory	RRID:IMSR_JAX:000,664
Mouse_CBA	The Jackson Laboratory	RRID:IMSR_JAX:000,656

Continued

REAGENT or RESOURCE	SOURCE	IDENTIFIER
Mouse_B6CBAF1	CBA ♂ x C57BL/6J ♀	N/A
Mouse_FVB/N	The Jackson Laboratory	RRID:IMSR_JAX:001,800
Mouse_129/Sv	The Jackson Laboratory	RRID:IMSR_JAX:000,691
Oligonucleotides		
Primers for qRT-PCR, see Methods S3	This paper	N/A
Probes for Wnt6/7b knockout, see Table S15	This paper	N/A
Recombinant DNA		
PB-TAC-ERP2	Addgene	Add80478
pDONR211	Invitrogen	12536017
pENTR-mCDX2	This paper	N/A
PB-CAG-Pbase	Gift obtained from Center for iPS Cell Research and Application, Kyoto University, Kyoto, Japan, (K. Woltjen lab)	N/A
PB-TAC-mCDX2-ERP	This paper	N/A
Software and algorithms		
FlowJo_v10.6.2	FlowJo™	RRID:SCR_008520; https://www.flowjo.com/
Prism 8	GraphPad	RRID:SCR_002798; https://www.graphpad.com
Fiji	NIH	https://imagej.net/Fiji
Excel	Microsoft	https://www.microsoft.com/nl-nl/microsoft-365/excel
SCOPE	N/A	https://scope.aertslab.org/
PTUI	N/A	https://bird2cluster.univ-nantes.fr/demo/PseudoTimeUI/human/PTUI.html
Burrows-Wheeler Aligner (BWA)	N/A	http://bio-bwa.sourceforge.net/
Integrative Genomics Viewer (IGW)	Broad Institute and the Regents of the University of California	https://software.broadinstitute.org/software/igv/
Deeptools	Max Planck Institute for Immunobiology and Epigenetics, Freiburg	https://deeptools.readthedocs.io/en/develop/
RStudio version 1.3.1056	RStudio	https://www.rstudio.com/products/rstudio/download/
Adobe Illustrator 2022	Adobe	https://www.adobe.com/products/illustrator.html
Adobe Photoshop 2022	Adobe	https://www.adobe.com/nl/products/photoshop.html

RESOURCE AVAILABILITY

Lead contact
Further information and requests for resources and reagents should be directed to and will be fulfilled by the Lead Contact, Nicolas C. Rivron, Ph.D. (nicolas.rivron@imba.oeaw.ac.at).

Material availability
This study did not generate new unique reagents.

Data and code availability
- The raw data of the scRNA-seq, bulk RNA-seq, and ATAC-seq reported in this paper have been deposited to the GeneExpression Omnibus (GEO) database and are publicly available as of the date of publication. Accession numbers are also listed in the key resources table. Microscopy data reported in this paper will be shared by the lead contact upon request.
- All original code has been deposited at Zenodo (https://doi.org/10.5281/zenodo.6602725) and is publicly available as of the date of publication. Link is listed in the key resources table.

● Any additional information required to reanalyze the data reported in this paper is available from the lead contact upon request.

EXPERIMENTAL MODEL AND SUBJECT DETAILS

Stem cells and culture condition

TSCs (F4 GFP and CDX2-eGFP TSCs which were a kind gift from Janet Rossant (Hospital for Sick Children, Toronto, ON, Canada; Department of Molecular Genetics, University of Toronto, Toronto, ON, Canada) and Jacqueline Deschamps (Developmental Biology and Stem Cell Research, Hubrecht Institute, Utrecht, Netherlands), respectively) were cultured following a previously published protocol (Kubaczka et al., 2014). Dishes were coated with 0.1% Matrigel, and cells were cultured in basal TX medium, which consists of DMEM/F12 (phenol red-free, with l-glutamine, or made in house, Media Lab IMBA, Vienna) supplemented with insulin (19.4 μg/mL), l-ascorbic-acid-2-phosphate (64 μg/mL), sodium selenite (14 ng/mL), sodium bicarbonate (543 μg/mL), and holo-transferrin (10.7 μg/mL). For TX culture, basal TX medium was further supplemented with FGF4 (25 ng/mL), TGFβ1 (2 ng/mL), and heparin (1 μg/mL). TXV cultured cells were plated on laminin 521-coated plates (10 ug/ml diluted in PBS without Mg^{2+} and Ca^{2+}) in basal TX medium supplemented with FGF4 (25 ng/mL), TGFβ1 (2 ng/mL), heparin (1 μg/mL), IL11 (50 ng/mL), Activin (50 ng/mL), Bmp7 (25 ng/mL), LPA (5 nM) and 8-Br cAMP (200 μM). Upon TSCs seeding (both in TX and TXV), Rock inhibitor (Y-27632, 2 μM) was added to help the attachment of TSCs onto the plates. TSCs were differentiated by changing the medium to basal TX medium without FGF4, TGFβ1 nor any other CDX2 regulator. This medium was maintained for 6 days.

TS medium cultured cells were plated on MEF in RPMI-1640 medium supplemented with 20% FBS, GlutaMax (1x, Gibco, 35,050,038), Sodium pyruvate (1x, Gibco, 11,360,070), HEPES (10 mM, made in house, Media Lab IMBA, Vienna), 2-Mercaptoethanol (100 μM, Gibco, REF 31350010), FGF4 (25 ng/mL), and heparin (1 μg/mL). ESCs (G4 WT ESCs which were a kind gift from Andras Nagy (Samuel Lunenfeld Research Institute, Mount Sinai Hospital, Toronto, ON, Canada; Department of Molecular Genetics, University of Toronto, Toronto, ON, Canada)), and H2B-RFP V6.5 sub-clone (V6.5 cell line was derived from C57BL/6 × 129/Sv background and obtained from the laboratory of Rudolf Jaenisch (The Whitehead Institute for Biomedical Research and Department of Biology, MIT, Cambridge, MA 02142, USA)) were cultured under 2i conditions B27N2 medium (Ying et al., 2008) in gelatin-coated plates without MEF. Cells were routinely passaged using either accutase or trypsin which was quenched with trypsin soybean inhibitor.

Mouse lines and embryos

All animal experiments (e.g., blastocyst flushing and uterus transfer) were conducted using 8–20-week-old female mice on a B6CBAF1 background, unless noted otherwise (e.g., C57BL/6J, FVB/N, and 129/Sv background for the TSCs derivation experiment). Mice were maintained at the IMP/IMBA animal house. All animal experiments were approved by the IMP/IMBA animal house and performed in accordance with the guidelines of the institution.

For the blastocyst flushing, super-ovulation was performed. Briefly, PMSG (5-6 IU per mouse, Hölzel Diagnostika, OPPA01037) was injected into females between 14:00-15:00h and followed by hCG injection (5-6 IU per mouse, MSD, Chorulon 1500 IU) within 47–48 h. Mice were mated on the same night hCG was injected (19:00-20:00h) and checked for plugs the next morning. Three or four days after checking the plug (for E3.5 or E4.5 blastocysts, respectively), the uterus was explanted and flushed with M2 medium (Millipore Sigma, MR-015P-D). For further culture of blastocysts, M2 or M2 supplemented with TXV factors (doubled concentration) were used for six or 20 h.

Six days after checking the plug (for E6.5 embryos), the uterine wall was gently removed with forceps. The deciduae were fixed with 4% formaldehyde overnight at 4°C and washed with PBS (three to four x for 1 h each). After EtOH-xylene-paraffin dehydration processing, the deciduae were embedded in paraffin and sliced to 2-μm thickness.

METHOD DETAILS

Generation of inducible Caudal Type Homeobox 2 overexpression cell lines

Inducible CDX2 TSCs were generated in the F4 TSCs line. pCAG-PBase (5 μg) and PB-TAC-*Cdx2*-ERP (5 μg) were transfected by NEPA21 electroporation (Nepa Gene Co. Ltd) into 1x10^6 cells in single-cell suspension. One day after transfection puromycin (1 μg/ml) was added for 7 days and the selected cells were maintained in a lower concentration of puromycin (0.1 μg/ml).

Generation of WNT6 and WNT7B knockout trophoblast stem cells

WNT6 and WNT7B KO TSCs were generated in the F4 TSCs line using a CRISPR-Cas9 system. Cells were electroporated (NEPA21 Super Electroporator, Nepa Gene Co., Ltd.) to transfect plasmids containing a specific guide RNA sequence (Figure S7D), as well as a Cas9, and BFP sequence. 10 μg of plasmid were used to transfect 1x10^6 cells. BFP positive cells were FACS sorted the next day. After their expansion, BFP negative cells were FACS sorted individually onto inactivated MEFs for clonal expansion and cultured in TXV medium. MEFs were depleted and cells were genotyped by Sanger sequencing. The effect of genomic editing on gene expression was confirmed by qRT-PCR using primers that amplify the 3′UTR and Western Blot (Figure S7E and S7F). Sequence information for all primers and sgRNAs used in this study are available in Methods S3.

Cell cycle analysis

After trypsinization, 1×10^5 TSCs and TESCs were incubated in 0.5 mL of TX medium with 10 ug/ml Hoechst 34580 for 30 min at 37°C. After the incubation time, tubes with cells were placed on ice and analyzed on a FACS Canto II.

Colony formation assay

Single cells were sorted into MEF coated plates with either TX or TXV medium. Medium was changed every 48 h and the number of wells containing colonies was assessed 7 days after sorting.

Combinatorial screen

A library of all compounds tested in the combinatorial screen can be found in Table S4. To identify positive modulators for CDX2 induction, CDX2-eGFP TSCs were cultured in TX medium for 24 h and then exposed to new TX media containing the different concentrations of individual compounds. After 48 h, CDX2 expressions of TSCs in each condition were analyzed by flow cytometry (FACS Fortessa, and FlowJo). For the experiment in Figure S3B, IGF2 (50 ng/mL) and ZSTK474 (PI3K inhibitor, 200 nM) were added to the medium.

Immunofluorescence

Samples were fixed using 4% formaldehyde in PBS for 20-30 min at room temperature (RT) followed by three washing steps with PBS. A 0.3% triton solution in PBS (PBS-T) was used for permeabilization for 30-60 min at RT, followed by a 1-2 h blocking step with 0.1% PBS-T + 2% BSA +3% serum (goat or donkey serum complementary to the host of the secondary antibody). Samples were then incubated overnight with the primary antibody diluted in blocking solution at 4°C. A detailed summary of all primary antibodies used in this study is provided in Methods S4. The next day samples were washed three times in 0.1% PBS-T and incubated with the corresponding secondary antibodies for 1 h at RT. Hoechst was used for counterstaining with or without WGA. Images were taken with one of the following microscopes: PerkinElmer Ultraview VoX spinning disk microscope, confocal Axio Observer inverted microscope equipped with a Yokogawa CSU X1 Spinning disk, and Olympus IX3 Series (IX83) inverted microscope equipped with a dual-camera Yokogawa W1 spinning disk. The images were analyzed with Fiji and photoshop.

Whole tissue staining/clearing and 3D imaging of embryos

After checking the expression of naive GFP in the chimeric embryos, we performed whole tissue staining and clearing as previously reported ((Kubaczka et al., 2014); Seong et al., 2018). Briefly, the dissected E6.5 embryos were incubated in Reagent 1 [25% (w/w) urea, 25% (w/w) N,N,N′,N′- tetrakis (2-hydroxypropyl) ethylenediamine, 15% (w/w) Triton X-100 in distilled water] for 3 days at 37°C, and washed with PBS (1 h) and with 0.1% Triton X-100 in PBS (PBS-T) (1 h × 2 times) at RT. The embryos were incubated with a blocking buffer (10% donkey serum in 0.5% PBS-T) overnight at 4°C, and then incubated for 4 days at 4°C with gentle rocking and the GFP, Elf5 antibodies (Methods S4). The embryos were incubated with fluorescent probes for 2 days at 4°C with gentle rocking, and Hoechst was used to detect nuclei. A PBS-T (0.3%) wash followed each antibody and Hoechst incubation (1 h × 3 times). The embryos were incubated in Reagent 2 [44% (w/w) sucrose, 22% (w/w) urea, 9% (w/w) 2,2′,2″-nitrilotriethanol, 0.1% (w/w) Triton X-100 in distilled water] for tissue clearing at least 1 day at 37°C with gentle rocking. Immunofluorescence was detected using an Olympus IX83 inverted microscope equipped with a dual-camera Yokogawa W1 spinning disk.

Single-molecule FISH

TSCs plated on glass coverslips were allowed to grow and subsequently fixed using RNase free 4% PFA in PBS +1% Acetic Acid for 20 min. After fixation, all samples were processed as described in the Quantigene ViewRNA kit instructions (Affymetrix, QVC0001). Briefly, after three washes with RNase free PBS, samples were incubated for 10 min in a detergent solution. This was followed by three washes with RNase free PBS after which samples were incubated for 5 min at RT with Q protease. Samples were again washed three times with RNase free PBS, and incubated with the probes of interest diluted in Probe set diluent at 40°C for 3 h (in a humidified chamber). After three washes with wash buffer, samples were incubated at 40°C for 30 min with a preamplifier diluted in amplifier diluent and washed again for three times. Samples were then incubated at 40°C for 30 min with amplifier diluted in amplifier diluent. Samples were washed again three times with wash buffer and incubated at 40°C for 30 min with label diluted in label probe diluent. After two washes, they were washed once more for 10 min. Samples were then incubated for 15 min in RNase free PBS with Hoechst and WGA as counterstains followed by three washes with RNase free PBS. Blastocysts or blastoids were carefully placed in mounting media in glass bottom 3.5 mm plates. All samples were imaged with a 63x oil immersion objective on a PerkinElmer Ultraview VoX spinning disk microscope.

Single-molecule FISH polarity quantification

Single molecule fluorescence *in situ* hybridization (smFISH) confocal images were taken with a z-step of 0.3 μm. Given the complexity of an analysis performed in 3D that would require an algorithm capable of segmenting cells and quantifying the number of transcripts in 3D, we decided to quantify a 2D projection of the slices that included the ICM and blastocoel. Those z stack projections were oriented with the polar side on the left and the mural side on the right and then analyzed for average column pixel intensity, allowing us to plot an average pixel intensity histogram. An intensity profile was plotted for each embryo and gene. Each blastocyst is structurally different showing distinct cavity sizes, which implies that a different percentage of the TE is in contact with the ICM for each embryo.

In order to compare the expression of polar and mural TE, we divided the length of the embryo in three segments of equal distance, irrespective of the total diameter. The intermediate segment was considered a transition stage between the polar and mural regions and therefore was not included in the next analyses. The polar and mural segments of the profile were analyzed by comparing the average pixel intensities of each pixel column included in the segment.

High content imaging
Each colony was imaged for E-CADHERIN, CDX2 and Nuclei stainings. E-CADHERIN staining was used for manual cell segmentation in ImageJ. Cell profiler was used for analysis of cell segmentation and the other stainings. Measurements obtained in the Cell profiler were used for further analysis using a Python pipeline. After discarding dividing cells based on the nuclear staining, a total of 502 control cells and 297 TXV TSCs cells were analyzed.

Live cell imaging
For the live cell imaging, CDX2-eGFP TSCs were seeded in glass bottom 12 well plates coated with Matrigel in TX medium at 25,000/cm2 density and they were incubated for 24 h at 37°C, 5% CO2. At the end of the 24h the medium was replaced with fresh medium and then the well plate was transferred to UltraVIEW spinning disk confocal microscope (PerkinElmer) for live imaging analysis. The stage area was set up to 37°C, 5% CO2 prior to the experiment. Images were collected every 12 min (5 timepoints per hour) for a total of 60 h in the GFP channels. The analysis of the live imaging data was completed with ImageJ.

Flow cytometry
Dissociated TSCs/TESCs with 0.05% trypsin were stained for 30 min on ice with the 100 ng of LY6A antibody, and were incubated on ice with anti-rat Alexa 647 (See Methods S4). Each antibody incubation was followed by a wash with FACS buffer (PBS plus 2% FBS). After resuspension of cells with FACS buffer, flow cytometry was conducted using FACS LSR Fortessa (BD). We used at least 10,000 cells for gating. Data was analyzed by FlowJo software. With CDX2-eGFP TSCs/TESCs, we directly used the cells for the flow cytometry after dissociation.

Blastoids made by H2B-RFP ESCs and CDX2-GFP TSCs (see 'Blastoids formation' section below) were dissociated with 0.05% trypsin. By plotting them with GFP and RFP, GFP$^+$ TR cells were sorted out for further analysis.

For CDX2-high, -low cell sorting, we dissociated CDX2-GFP TSCs and sorted the cells with FACS aria III based on naive GFP signal. For CDX2-high and -low groups (H and L), we use top and bottom 10% of GFP$^+$ cells, respectively.

qRT-PCR
RNA was harvested using either the RNeasy Mini Kit (Quiagen, 74,104) or the innuPREP RNA Mini Kit 2.0 (Analytik Jena, 845-KS-2040050) according to the manufacturer's instructions. For cDNA synthesis RNA was incubated with 2.5 μM OligodT primer (New England Biolabs, S1316S) and 0.5 μM dNTPs (in house, Molecular Biology Service IMBA Vienna) at 65°C for 5 min. Reverse transcription was then performed using the SuperScript™ III Reverse Transcriptase (Invitrogen, 18,080,044) together with RNaseOUT™ Recombinant RNase Inhibitor (Invitrogen, 10,777,019) according to the protocol provided by the manufacturer. For the qPCR reactions GoTaq qPCR Master Mix (Promega, A6001) was used. All qPCRs were performed using a Bio-Rad CFX Connect Real-Time PCR System. Relative expression levels of target genes were calculated with the ΔΔCT method using *Hprt* as an endogenous reference gene for internal normalization. Sequence information for all primers can be found in Methods S3.

RNA sequencing
For bulk sequencing 1000 control and TXV cultured cells were used for Trizol RNA extraction. Both bulk and single cell sequencing was performed following the Cel Seq 2 protocol (Hashimshony et al., 2016). In-bulk samples were first normalized and then analyzed using the DESeq2 package in Rstudio. Triplicates for each group (F4 GFP in TX TXV, TX differentiated, and TXV differentiated) were analyzed. Genes were considered differentially expressed when showing a 1.5-fold expression change with a p value < 0.05. The DAVID gene ontology online tool was used for gene enrichment analysis.

Mapping and processing of single-cell mRNA sequencing data
Read one contains the cell or section barcode and the unique molecular identifier (UMI). Read two contains the biological information. Reads 2 with a valid cell barcode were selected and mapped using STAR-2.5.3a with default parameters to the mouse mm10 genome, and only reads mapping to gene bodies (exons or introns) were used for downstream analysis. Reads mapping simultaneously to an exon and to an intron were assigned to the exon. For each cell or section, the number of transcripts was obtained as previously described (Grün et al., 2014). We refer to transcripts as unique molecules based on UMI correction.

Analysis of single-cell mRNA sequencing data
To analyze CEL-Seq single cell sequencing experiments, mouse genomic sequence and annotation from NCBI GRCm38.p6 were used. Reads were trimmed using trim_galore v0.6.4 and subsequently aligned to the mouse genome (GRCm38.p6) using STAR v2.7.6a. UMI quantification and raw count matrixes generation were performed using umi_tools v1.0.1.

Further analysis was performed in R v4.0.4 with Seurat v3.2.3. Cells with a number of genes comprised between 200 and 2500 or with ≥ 5% mitochondrial genes were retained. Standardization of per gene expression values through the cells was performed using

NormalizeData, FindVariableFeatures and ScaleData; top 2000 variable genes were selected. Principal Component analysis was performed with RunPCA function whereas clusters were identified using FindNeighbours and FindClusters at a resolution of 0.8. Cluster marker genes and differentially expressed genes were detected with the Wilcox likelihood-ratio test using the FindMarkers function with logfc.threshold = 0.1. Uniform Mani-fold Approximation and Projection was used for the visualization.

Gene enrichment analysis was performed using GSEA V4.1.0 using the preranked function. Cluster genes identified using FindMarkers from the Seurat package were ranked according to the p value and the log fold change before conducting the gene enrichment analysis. Gene sets used in the preranked GSEA were obtained by performing differentially gene expression (as described above) between annotated polar and mural cells at the 4.5 blastocyst stage by (Nakamura et al., 2015) (GSE63266) and TE and ExE by (Posfai et al., 2021) (GSE145609). For the latter, annotations were kept as provided by the authors meaning that we included single TE cells from E2.5, E2.75, E3.0, E4.5 and ExE cells from E7.0 and E7.5 in our analyses.

Data was analyzed using the monocle and RaceID pipelines (Grün et al., 2014; Grün et al., 2016; Posfai et al., 2021) to organize cells into pseudotime trajectories (Trapnell et al., 2014) and generate unsupervised clustering heatmaps.

Caudal Type Homeobox 2 ChIP-seq analysis

Publicly available datasets for CDX2 ChIP-seq (GSM2412032), the corresponding input control (GSM2412036), and chromatin accessibility (ATAC-seq, GSM2412027) for mouse TSCs were reanalyzed. Briefly, raw sequencing reads were trimmed using Trim-momatic SE for Truseq2:SE adapters and were aligned to mouse mm10 reference genome using default parameters of Burrows-Wheeler Aligner. BigWig files were generated utilizing the bamCoverage function using RPKM normalization from deepTools 3.3.2. Reads from input signals were subtracted using bamCompare utilities. Normalized reads for both ChIP-seq and ATAC-seq were used for visualization with Integrative Genomics Viewer (IGV).

Chromatin immunoprecipitation PCR (ChIP-PCR)

Chromatin immunoprecipitation was performed using the ChIP-IT High Sensitivity kit (Active Motif, cat no 53040 version A6), following the included protocol. Briefly, the frozen cell pellets were resuspended in Chromatin Prep Buffer and nuclei isolated by douncing for 40 times on ice using a tight-fitting pestle. Samples were placed in an ice bath and sonicated to a size range of 200–800 base pairs using a probe sonicator. Input chromatin was prepared by treating a sample of the sonicated chromatin with RNAse A and Proteinase K, followed by de-crosslinking at 80°C for 2 h. The de-crosslinked DNA was precipitated using ethanol and the Pre-cipitation Buffer and Carrier included in the kit, spun down, washed with 70% ethanol and resuspended in DNA Purification Elution Buffer (included in kit). Chromatin immunoprecipitation was performed using 0.7–2.5 μg chromatin and 4 μg anti-H3K9Ac (Active Motif 61,251) or anti-H3K4Me3 (Diagenode C15410003) antibody. After overnight incubation at 4°C with rotation, the reactions were incubated with Protein G agarose beads (included in kit) for 3 h at 4°C with rotation to capture the antibody/chromatin com-plexes. The beads were recovered and washed five times using the columns and wash buffer included in the kit, and the bound chro-matin eluted twice using the included elution buffer. The eluded chromatin was treated with Proteinase K and de-crosslinked at 80°C for 2 h, after which the DNA was purified using the included purification columns and recovered in a 200 μL elution buffer (included).

qPCR was carried out on a BioRad CFX machine using a SYBRgreen based master mix. The amount of precipitated chromatin as a percentage of input for each analyzed region was determined using standard curves created from input chromatin in amounts ranging from 0.005 ng to 50 ng. Primer sequences are listed in Methods S2.

Chimeric embryo formation

Defrosted 8-cell embryos (Janvier Lab, Quickblasto) were cultured in KSOM medium (Sigma, MR-101D) for 4-5 h (37°C, 5% CO2). A micromanipulator was used to inject 8-12 F4 GFP TESCs or TSCs into the morula or early blastocyst cavity with the aid of a laser (Hamilton Throne, Xyrocos). TSCs/TESCs injected blastocysts were then transferred into the uterine horns of E2.5 pseudopregnant females. A maximum of seven blastocysts were used per horn. E6.5 embryos were isolated in PBS by gentle dissection and fixed with 4% formaldehyde. The embryos were stained using whole tissue staining and clearing methods described below.

Trophoblast stem cells line derivation and staining

E3.5 blastocysts were isolated from pregnant females. Zona pellucida was removed using Tyrode's acid solution before placing them in MEF-coated plates with TS, TX, or TXV medium. The medium was changed every 48 h. The outgrowth was monitored daily and was passaged on day 5–7 depending on cell growth. With proper size, the colonies were fixed, and immunofluorescence was performed as described above.

For TSCs line derivation from E6.5 conceptus in TXV medium, we isolated the ExE from E6.5 conceptus by manually cutting off the EPI, EPC, and visceral endoderm. The ExEs were placed on MEF in TXV medium, and the medium was changed every 48 h. The outgrowths were dissociated after 2 to 3 days and colonies became visible within the next 5 days. Both E3.5 and E6.5-derived TSCs were cultured on MEF for three passages, and then transferred to laminin-coated plates.

Blastoid formation

Full protocol link: https://protocolexchange.researchsquare.com/article/nprot-6579/v1). Agarose microwell arrays were casted us-ing a custom PDMS stamp and incubated overnight in mES serum containing media. After washing the chips with PBS, an ESC so-lution of 150k cells/ml was dispensed in the central chip and allowed to settle. After 20 min, an additional 1 mL of mES medium was

added. 24-28 h later, mES medium was removed and a TSCs/TESCs solution of 150k cells/ml was dispensed. After allowing the cells to fall in the microwells, 1 mL of blastoid media was added to the wells. WNT7B or WNT6 KO blastoids were made from normal ESCs and WNT7b or WNT6 KO TSCs. The rest of the procedure was the same as the general protocol.

mES medium is DMEM high glucose medium (made in house, Media Lab IMBA, Vienna) supplemented with 10% FBS, GlutaMax (1x, Gioco, 35,050,038), Non-essential amino acid (1x, Gibco, 11,350,912), HEPES (10 mM, made in house, Media Lab IMBA, Vienna), 2-Mercaptoethanol (100 μM, Gibco, REF 31350-010), LIF (1000 U/ml, Sigma, ESG1107), and 1x Penicillin/streptomycin (Gibco, 15,140,122). Blastoid medium consisted of 50% basal TX medium and 50% WNT3A conditioned medium supplemented with 20 μM Y-27632 (MedChem Express, HY-10583), 3 μM CHIR99021 (MedChem Express, HY-10182), 1 mM 8-Br cAMP (BIOLOG, B 007-500), 25 ng/mL FGF4 (R&D systems, 5846F4), 15 ng/mL TGFβ1 (Peprotech 100-21), 30 ng/mL IL11 (Peprotech, 220-11), 1 μg/mL heparin (Sigma-Aldrich, H3149) and 1x Penicillin/streptomycin (Sigma, P0781). An additional shot of 8-Br cAMP was added to each well 24 h after TSCs/TESCs seeding to add another 1 mM per well. Blastoids were analyzed 65 h after TSCs/TESCs seeding unless noted otherwise.

To culture EPSCs and to make blastoids formed from the association of EPSC and TESCs, we followed the variation on our initial protocol as described in the reference (Sozen et al., 2019), at the exception of the initial TSCs culture conditions that were replaced by TESCs.

Uterus transfer and decidua analysis

Four hours before uterus transfer, the blastoid medium was replaced with DMEM high glucose medium. Picked blastoids from the microwells were placed on four ring-well plate and briefly washed with DMEM high glucose medium. With the few medium, 10-12 blastoids were transferred into the only one of the uterine horns of E3.5 pseudopregnant females, unless noted otherwise. E7.5 deciduae were explanted 4 days after uterus transfer. The bulb which has a clearly bigger diameter than the width of a normal uterus was considered as a decidua, and the number of deciduae was confirmed by three different scientists by performing blind test. We took decidua pictures with the ruler, and measured the length of deciduae from mesometrium side to anti-mesometrium side (perpendicular to the direction of the cervix from the ovary) with Fiji.

For the fixed blastoids transfer, blastoids were fixed with 4% formaldehyde in PBS for 30 min at RT. The blastoids in the control group were in the PBS for 30 min to be fair. After enough washing with PBS, the blastoids were transferred. For the Cdx2i blastoids, 225 nM (100 ng/mL) of doxycycline was added when the TSCs were seeded on the microwells with a blastoid medium. For the blastoids with GW501516, 3 μM of GW501516 was added 1 day before the uterus transfer (around 40-45 h after TSCs seeding).

For the comparison experiment of blastocysts with TSCs and TESCs blastoids, freshly isolated E3.5 blastocysts from pregnant females were directly transferred into the E3.5 pseudopregnant recipients. For IWP2 treatment before uterus transfer, we cultured eight cell-embryos in KSOM either with or without IWP2. After 2 days, they developed late blastocysts (E4.0-E4.5) and were transferred to the uterus.

Blue band assay

Two days after uterus transfer, 0.4% trypan blue (Thermofisher Scientific, T10282, 10 μL per 1g of mouse weight) was injected through intravenous (i.v.) injection. After 30 min, the mice were sacrificed and E5.5 uteri were analyzed. For Figure 7C, only four to six blastocysts were transferred to prevent overlap of individual blue bands.

Western Blot

For protein isolation, TSCs were lysed using RIPA buffer (Thermo Fisher Scientific, 89,900). For western blotting, proteins were transferred to 0.2μm Nitrocellulose membranes (Bio-Rad, 1,620,112), and membranes were then blocked with 0.1% PBS-T (PBS plus 0.1% Triton X-100) containing 5% skim milk at RT for 1 h. To detect specific proteins of interest, WNT7B and a-TUBULIN antibodies were used (See Methods S4). Horseradish peroxidase (HRP)-conjugated secondary antibodies were then used. Each antibody incubation was followed by washing with 0.1% PBS-T. Luminescence was detected with a Bio-Rad ChemiDoc MP Imaging System.

SCOPE and PTUI

Wnt family expression levels in the mouse embryo were analyzed with SCOPE (https://scope.aertslab.org/) using data resources from (Posfai et al., 2021) (GSE145609) for the analysis of transcriptomic differences between the TE and ExE. Wnt family expression levels in the human embryo were analyzed with PTUI (https://bird2cluster.univ-nantes.fr/demo/PseudoTimeUI/human/PTUI.html) by using data resources from ().

QUANTIFICATION AND STATISTICAL ANALYSIS

Statistical analyses were performed using GraphPad Prism 8 (GraphPad Software) and Excel (Microsoft). All error bars represent the SEM(SEM). Data were analyzed using a one-way ANOVA, a two-tailed t-test (for a difference in means), Mann-Whitney analysis, or Wilcox likelihood-ratio test. The statistical analysis used for each dataset is indicated in the figure legend. A p value < 0.05 was considered statistically significant at the 95% confidence level. The number of biological (non-technical) replicates for each experiment is indicated in the figure legends. All representative images shown are from experiments that have been performed in triplicate at least, except Figure S4H (two independent experiments with pooled 36-40 embryos).